Journal of Volcanology and Geothermal Research 382 (2019) 233–252

Contents lists available at ScienceDirect

Journal of Volcanology and Geothermal Research

journal homepage: www.elsevier.com/locate/jvolgeores

Construction of probabilistic event trees for eruption forecasting at Sinabung volcano, Indonesia 2013–14

Heather M.N. Wright [a,*], John S. Pallister [a], Wendy A. McCausland [a], Julia P. Griswold [a], Supriyati Andreastuti [b], Agus Budianto [b], Sofyan Primulyana [b], Hendra Gunawan [b], 2013 VDAP team, CVGHM event tree team:

Maurizio Battaglia, Angie Diefenbach, Julia Griswold, John Ewert, Peter Kelly, Christoph Kern, Martin LaFevers, Andy Lockhart, Jeff Marso, Gari Mayberry, Wendy McCausland, John Pallister, Steve Schilling, Rick Wessels, Randall White, Heather Wright

Nurnaning Aisyah, Supriyati Andreastuti, Agus Budianto, Anjar Heriwaseso, Nugraha Kartadinata, Kristianto, Sofyan Primulyana, Raditya Putra, Ugan Boyson Saing, Agus Solihin, Yasa Suparman, Devy Damil Syahbana, Hetty Triastuty

[a] Volcano Disaster Assistance Program, U.S. Geological Survey, 1300 SE Cardinal Court, Vancouver, WA 98683-9589, USA
[b] Center for Volcanology and Geologic Hazards, Diponegoro 57, Bandung, Java 40122, Indonesia

ARTICLE INFO

Article history:
Received 9 June 2017
Received in revised form 29 January 2018
Accepted 6 February 2018
Available online 8 February 2018

Keywords:
Eruption forecast
Volcano hazards
Probabilistic forecast
Volcanic dome
Andesite volcano

ABSTRACT

Eruptions of Sinabung volcano, Indonesia have been ongoing since 2013. Since that time, the character of eruptions has changed, from phreatic to phreatomagmatic to magmatic explosive eruptions, and from production of a lava dome that collapsed to a subsequent thick lava flow that slowly ceased to be active, and later, to a new lava dome. As the eruption progressed, event trees were constructed to forecast eruptive behavior six times, with forecast windows that ranged from 2 weeks to 1 year: November 7–10, December 12–14, and December 27, 2013; and January 9–10, May 13, and October 7, 2014. These event trees were successful in helping to frame the forecast scenarios, to collate current monitoring information, and to document outstanding questions and unknowns. The highest probability forecasts closely matched outcomes of eruption size (including extrusion of the first dome), production of pyroclastic density currents, and pyroclastic density current runout distances. Events assigned low probabilities also occurred, including total collapse of the lava dome in January 2014 and production of a small blast pyroclastic density current in February 2014.

1. Introduction

August–September 2010 marked the first historic eruptions at Sinabung volcano, Indonesia (Fig. 1), producing ash columns to 5 km asl and prompting evacuation of surrounding communities (Hendrasto et al., 2012). Renewed unrest (Gunawan et al. 2019) in 2013 was again accompanied by eruptions beginning September 15, 2013. The ensuing eruption sequence has included phreatomagmatic eruptions, explosive magmatic eruptions, and persistent lava effusion that continues to the time of this writing (May 2017). In late 2013, as eruption frequency increased, seismicity increased, and SO_2 continued to be detected, scientists from the joint USAID – U.S. Geological Survey (USGS) Volcano Disaster Assistance Program (VDAP) and the Center for Volcano and Geological Hazard Mitigation, Indonesia (CVGHM; a division of the Indonesian Geological Agency (GA)) began to use probabilistic event tree analysis as a forecasting tool. This tool has been used six times since re-initiation of eruptions in 2013. Here, we evaluate the utility of these event trees in forecasting eruptions and in documenting the basis for forecasts. We follow Siebert et al. (2010) and GVP (2013) in defining an eruption as the arrival of volcanic products at Earth's surface. Eruptions can be explosive or effusive. We use the phrase 'eruption sequence' to encompass periods

* Corresponding author.
E-mail address: hwright@usgs.gov (H.M.N. Wright).

https://doi.org/10.1016/j.jvolgeores.2018.02.003

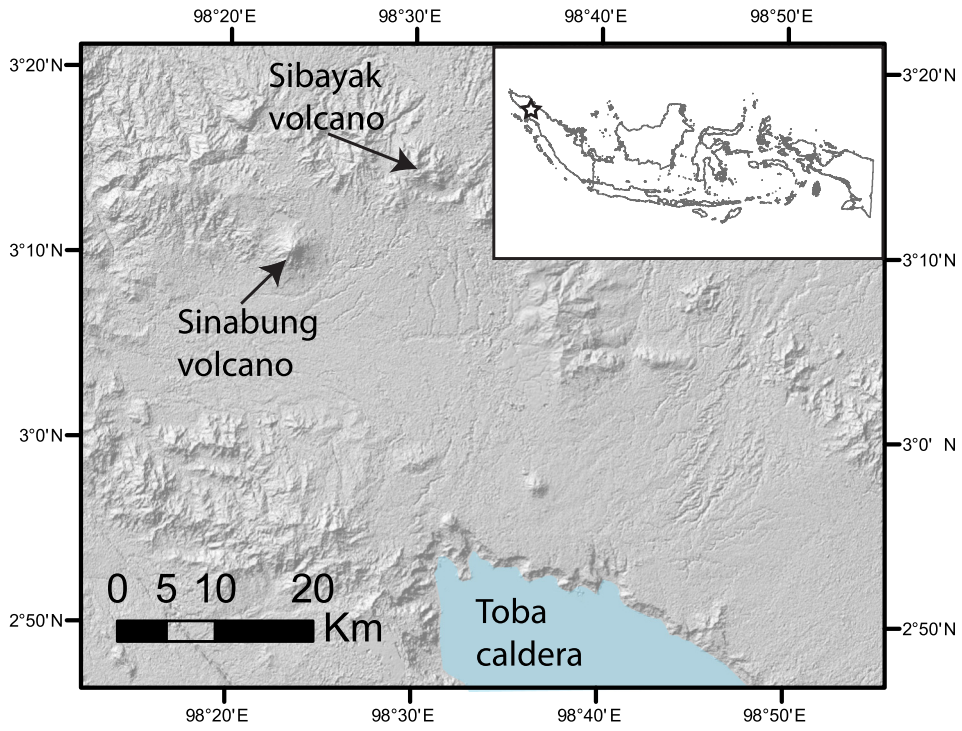

Fig. 1. Hillshade map showing the location of Sinabung volcano, NW of the Toba caldera in North Sumatra. The inset map shows the country of Indonesia with the star indicating the location of Sinabung volcano.

of eruptive activity, within which individual explosive eruptions and/or effusions of varying duration may occur.

1.1. Event trees

Event trees present a logical framework for examination of the possible outcomes of volcanic unrest and for characterizing their relative likelihoods (Fig. 2; Newhall and Hoblitt, 2002). Early in the tree (on the left side of Fig. 2) each branch originating from a single fork presents a mutually exclusive possible scenario of eruptive activity. As you progress down a single limb of the tree (toward the right side of Fig. 2) into the phenomena and distance columns, paths are no longer mutually exclusive, because multiple hazardous phenomena can be produced in a single eruption. Two probabilities are shown, one above the other, at each event on the tree. The conditional probability (the lower probability on Fig. 2, labeled "cond.") is the probability of an event given that the previous event has occurred. The product of this conditional probability and the probability that the previous event occurred results in the nodal probability of that outcome, or the value shown in the outlined box at that node (Fig. 2).

Since the original application of event trees to forecasts of post-climactic eruption hazards and risk at Mount St. Helens in 1980 (Newhall, 1982), many observatories have adopted a similar framework for quantifying hazard probabilities (e.g., Aspinall, 2006; Neri et al., 2008; Lindsay et al., 2010). Furthermore, a common feature of event trees is the use of Bayesian statistics, whereby updates to forecast probabilities are made when new information is made available. Estimation of event probabilities relies on a combination of local eruptive history, global comparisons with analog volcanoes, integration of current monitoring data, and elicitation of expert opinion. The nature of expert elicitation differs between scientific and organizational groups, but is required in all operational instances of event tree use. For example, at Soufrière Hills volcano, eruptive scenarios are discussed among a group of experts whose probability estimates are combined using a performance-based calibration determined from a series of seed questions (Aspinall, 2006). In contrast, at Vesuvius volcano, eruption probabilities during unrest are calculated using an event tree framework, where thresholds in monitoring data are determined a priori by expert elicitation to indicate unrest or likely eruption. Event probability density functions are then calculated for updated monitoring values by extrapolation between threshold limits (Marzocchi et al., 2004). A further version of the event-tree method requires discussion and group consensus to arrive at event probabilities. This "multiple data sets" method is used by VDAP, commonly during crises for which there may be limited prior information and a need to reach a rapid consensus among observatory scientists (Newhall and Pallister, 2015). Event trees have been used jointly by VDAP and CVGHM for eruption forecasting in Indonesia previously: including in the Merapi 2006 crisis (Pallister et al., 2013b) and outside of crisis at Soputan volcano (Kushendratno et al., 2012). This is the method that was used in partnership with CVGHM colleagues to forecast eruptions at Sinabung volcano in 2013–4.

1.2. Sinabung volcano

Sinabung volcano is located in Karo Regency, north Sumatra, ~30 km northwest of Toba caldera and ~15 km southwest of Sibayak stratovolcano (Fig. 1). Sinabung experienced its first historic eruption in August 2010, followed by six additional eruptions into September 2010 (Hendrasto et al., 2012). All ash emissions were purely phreatic, with ash columns that rose to 5 km above the summit, and that were derived from two distinct vents (Iguchi et al., 2011). In late September, activity declined to production of steam plumes and the eruption sequence effectively terminated.

For the subsequent three years, the volcano entered a period of relative repose, producing persistent fumarolic emissions and continued swarms of distal volcano tectonic (VT) earthquakes through the onset of the current eruptive sequence beginning September 15, 2013 (Gunawan et al. 2019). Since that time, eruptions have produced explosive columns, disperse tephra, crater-limited lava domes, flank-descending lava flows, vent-derived pyroclastic density currents (PDCs), and lava flow margin collapse-generated PDCs (Gunawan et al. 2019). Based on changes in style of eruption and nature of eruptive

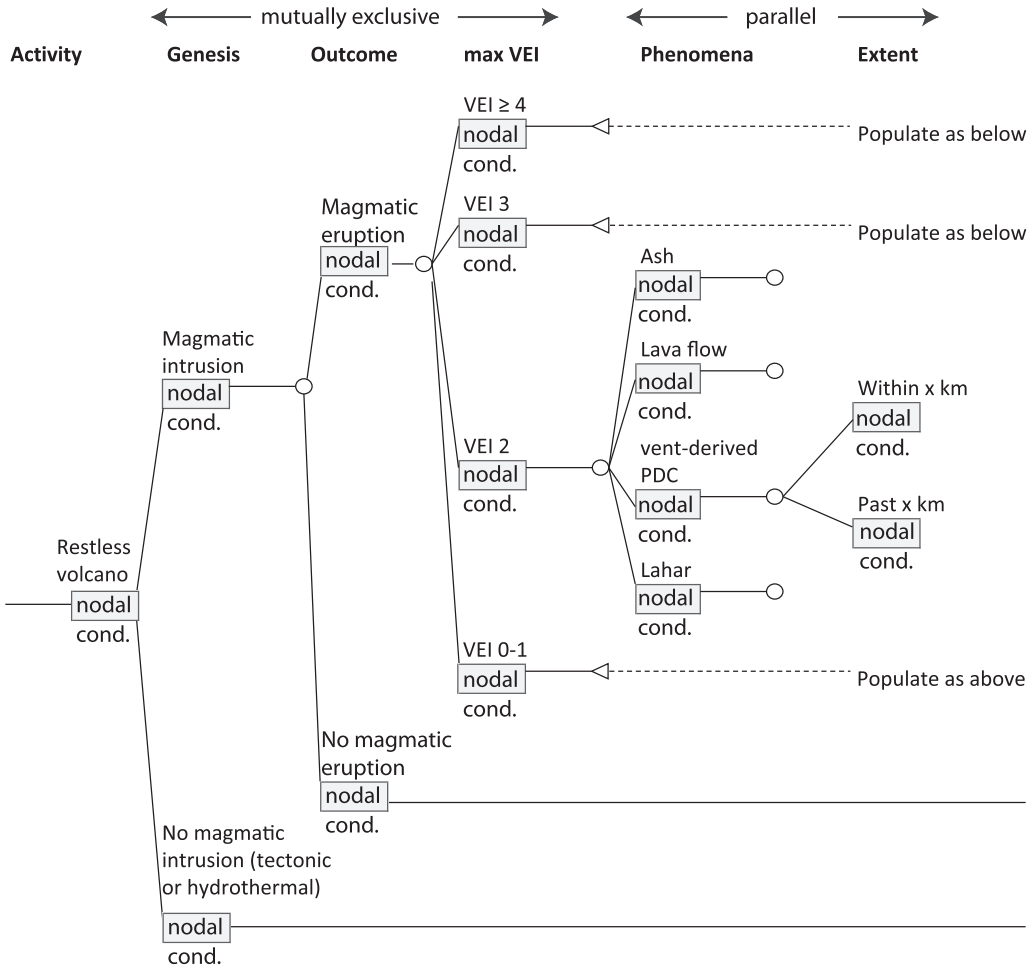

Fig. 2. A generic event tree, modified from Newhall and Hoblitt (2002), here including hazards, but not risk. Mutually exclusive scenarios must have conditional probabilities that sum to 100% on a single branch. Parallel limbs can occur simultaneously; therefore probabilities do not necessarily sum to 100%. Conditional probabilities (probability of occurrence given that the previous has already happened) are abbreviated here as 'cond.', nodal probabilities are listed within boxes, here denoted 'nodal'.

products, Gunawan et al. (2019) divide the current eruptive sequence into five stages that extend to the time of this writing (May 2017). These phases include: I) a phreatomagmatic phase (July 2013–18 December 2013); II) an initial lava dome extrusion and collapse phase with south- and southeast-directed PDCs (block-and-ash flows and related surges) (18 December 2013–10 January 2014); III) a southeast flank descending lava-flow and collapse phase (10 January 2014–mid-September 2014); IV) a second lava dome and collapse phase producing south- and southeast-directed PDCs (mid-September 2014–July 2015); and finally V) a lava dome collapse and ash explosion phase with PDCs directed to the southeast and east (August 2015–present).

2. Approach

Event trees were constructed six times in 2013–4 (Table 1). Construction of new short-term trees was triggered by changes in the character of monitoring data, but new trees were not always constructed before the expiration of the previous forecast/event tree. Dates of tree construction were: November 7–10, December 12–14 and December 27, 2013; and January 9–10, May 13, and October 7, 2014, where date ranges indicate that population of the event tree was not completed in a single day (Table 1). Forecast windows ranged from 2 weeks to 1 year, where the choice of forecasting window depended upon operational requirements. Here, we present all of the event trees constructed over this period. We evaluate the format of trees (which changed throughout the interval), the content included in the trees (including monitoring data and global analogs), and compare forecasts with reality. We also present a series of highlighted research questions for which answers would have helped us better evaluate event probability.

Table 1
Summary of event tree forecasts.

Event tree date	Duration of forecast	Most likely maximum VEI
Nov. 10, 2013	2-Week	2
Dec. 12–14, 2013	1-Month	2–3
Dec. 27, 2013	1-Month	2–3
Jan. 10, 2014	3-Week	2 and small dome collapses
May 13, 2014	1-Month	2–3 with small dome collapses
October 7, 2014	1-Year	2–3 with small dome collapses

The construction and population of event trees during a crisis involves several steps. For short term event trees, all of these steps need to occur within a limited time frame in order to maximize forecast utility – ideally within a single day, but at Sinabung, the process took up to 3 days (trees with a listed date range). In VDAP's application of event trees, the format of the tree is first chosen, where a generic format (Fig. 2) can be modified to reflect additional event scenarios. Second, the duration of the tree is chosen based upon the operational needs of the partner observatory. Short-term trees (weeks) are most useful for communication with the local population about immediate hazards and short-term evacuations, whereas medium-term trees (years) are more useful for assessment of staffing needs, permanent relocation of population, and evaluation of land use. Third, scientists gather relevant monitoring data and background information in order to share these data with the discussion group. Fourth, scientists meet (in person and remotely) to discuss data,

with particular focus on changes in monitoring parameters and their relative rates of change. Through interpretation and integration of these data, the group arrives at a single consensus probability (or a stated range of probabilities, see Section 4.3.4 Incorporation of uncertainty, below) for each node of the tree. Conditional probabilities at each node are multiplied by parent probabilities in order to calculate the nodal probability of each event (Newhall and Pallister, 2015).

Probabilities in event trees are semi-quantitative. In order to minimize over-precision, we populated the event trees with whole numbers. Importantly, uncertainty was not quantified in the event trees presented here, except through inclusion of a range of probabilities when consensus could not be achieved. In general, consensus probabilities are intended to provide robust relative measures of hazard and to achieve order-of-magnitude quantification of likelihood consistent with individual's risk tolerance resolution (cf. Newhall and Hoblitt, 2002). We assign probabilities of 95% to events that are almost certain, 70% to those that are more likely than not to occur, and 50% to those that have a roughly equal probability of occurrence and non-occurrence. Probabilities between these bounding values are then assigned based our group's discussion of global data and on local geologic and monitoring data. This semi-formal translation scheme between verbal phrases and numerical probabilities reflects the hazard perceptions of our group and differs in specifics from other translation schemes (e.g., IPCC treatment, Mastrandrea et al., 2011). A translation table is not, however, universally applied in communication of event tree results (cf. need for tailored formal translation tables in volcanology dependent upon the community, Doyle et al., 2014).

Nodes (junctions in tree limbs) are numbered and correspond to numbered text in a separate sheet that documents the basis for probabilities in the event tree spreadsheet (Supplementary Data). For the Sinabung event trees, the forecast probabilities relied heavily on local monitoring data, using global information to fill in gaps in knowledge. Monitoring data included seismic, geodetic, gas, and satellite-derived data and field observations. Short-term event trees relied exclusively upon interpretation of monitoring data to evaluate outcome (eruption vs. no eruption) probabilities (Fig. 2). In contrast, eruptive explosivity probabilities were estimated based on a combination of inputs, including the local eruptive history at the volcano, the global record of volcanic eruption sizes, and an interpretation of monitoring data. The past history of the volcano and the global distribution of eruption sizes formed the background explosivity distribution (akin to the prior probability distributions in a Bayesian framework). Monitoring data then influenced this distribution by affecting our interpretation of fundamental processes of magma degassing and ascent using a conceptual model. References to each input information source and documentation of thought logic were captured in the event tree file. In addition, this file documented remaining questions, possible data gaps, or gaps in our knowledge about global analogs. Here, we highlight the results of event tree construction through a representative selection of event tree probabilities and the data that support them.

3. Application of event trees

3.1. November 7–10, 2013 tree

The first event tree constructed in this sequence was started on November 7 and completed on November 10, 2013 (Figs. 3 and 4), almost two months after re-initiation of eruptive activity on September 15, 2013 (Fig. 3a). Construction of the event tree was prompted by growing concern over an increase in activity, as reflected in seismicity, gas emissions, and character of summit eruptions. This tree was constructed by the VDAP team as a means to remotely assist the CVGHM crisis response team and to begin a more comprehensive analysis of the hazards. As documented in this tree, activity included the increasing frequency of small (VEI 1) emission events beginning October 23, the occurrence of small pyroclastic density currents beginning November 3, an increase in SO_2 emission rates from 128 tons/day on September 16 to 814 tons/day on October 26 (SO_2 emission rate had actually reached 1242 tons/day by November 8; Primulyana et al., 2019; but that information was not available at the time this tree was created), the continued occurrence of distal and deep VT earthquakes since September (dVTs indicate pressurization of a magmatic system, White and McCausland, 2016; White and McCausland, 2019), the presence of hybrid and low frequency (LF) seismicity starting November 2, and the presence of tremor starting in mid-October (McCausland et al. 2019). The time window for this forecast was set at two weeks, due to the increasing concern about the risk to surrounding communities, including thousands of residents within 5 km of the summit (Andreastuti et al. 2019). For node 2 (Fig. 4), based exclusively on the relative increase in monitoring parameters (ash emissions, gas emissions, persistence of deep and distal VT seismicity), we therefore assigned a probability of 70% for continued eruptions within the following two weeks (node 2, Fig. 4).

The probability distribution of event explosivity/magnitude (VEI) (node 4, Fig. 4) incorporated the pre-historic eruptive history at Sinabung as inferred from geologic mapping and volcaniclastic stratigraphy, the global context for eruptions from andesitic stratovolcanoes worldwide, and local monitoring data (e.g., seismicity types and rates, gas emission rates, geodetic changes, observations of the lava dome and for later trees, estimation of dome extrusion rates). Geologic mapping at Sinabung by Iguchi et al. (2012; and by Prambada et al. 2010, although this work was unknown to the VDAP group until creation of the second event tree on December 12–14) indicated that the youngest stage of volcanic activity at Sinabung is dominated by production of porphyritic 2-pyroxene basaltic andesite to hornblende 2-pyroxene andesite lava flows and pyroclastic deposits. The most common eruption style included dome-forming lava extrusion associated with block and ash flows (dense PDCs, generated by dome or lava collapse); no Subplinian or Plinian tephra deposits have been recognized, however tephra deposits are easily eroded in Indonesia, and so may be underrepresented in the depositional record. Therefore, we assigned a relatively low, 20% conditional probability that eruptions would be VEI ≥ 3, 55% to VEI 2, and 25% to VEI 0–1, based on eruptive history alone (node 4, Fig. 4).

Further, we queried the Smithsonian's GVP catalog (Global Volcanism Program, 2013) for all eruptions within Indonesia, which documents 37 VEI ≥ 4 eruptions, 152 VEI 3; 888 VEI 2; and 297 VEI 0–1; or 13% VEI ≥ 3; 65% VEI 2; and 22% VEI 0–1. Finally, the monitoring data, including increasing gas emission rates and increasingly energetic VT swarms, indicated that more eruptions were likely, possibly of larger size than seen so far. However, there were no signs of significantly large pressure increases or unusually rapid magma ascent. These various data streams (local and global) all indicated that the most likely maximum eruption explosivity was VEI 2.

Consistent with the most likely path through the tree, within the two-week forecast window eruptions continued, producing explosive eruptions with a maximum VEI of 2 (VEI ranged from 1 to 2). Therefore, we focus on the VEI 2 limb of the tree for a comparison between forecast phenomena and reality. No dome was extruded within the 2-week period ending November 24 (25%/10% conditional/nodal probabilities for dome extrusion associated with a VEI 2). Ash fall did take place (100%/39% conditional/nodal probabilities for VEI) and small pyroclastic density currents with runout distances up to 3 km (5%/2% conditional/nodal) also took place. In retrospect, the principal value of this tree was in emphasizing the high probability of continued eruptions and that the most likely maximum magnitude of eruptions was VEI 2.

3.2. December 12–14, 2013 tree

The first phreatomagmatic eruption occurred on November 11, 2013 (Andreastuti et al. 2019; Nakada et al. 2019), followed by a 12-km high plume on November 23, when CVGHM changed the alert level to Level 4 (AWAS), its highest level (Fig. 3a). Most eruptions in late November

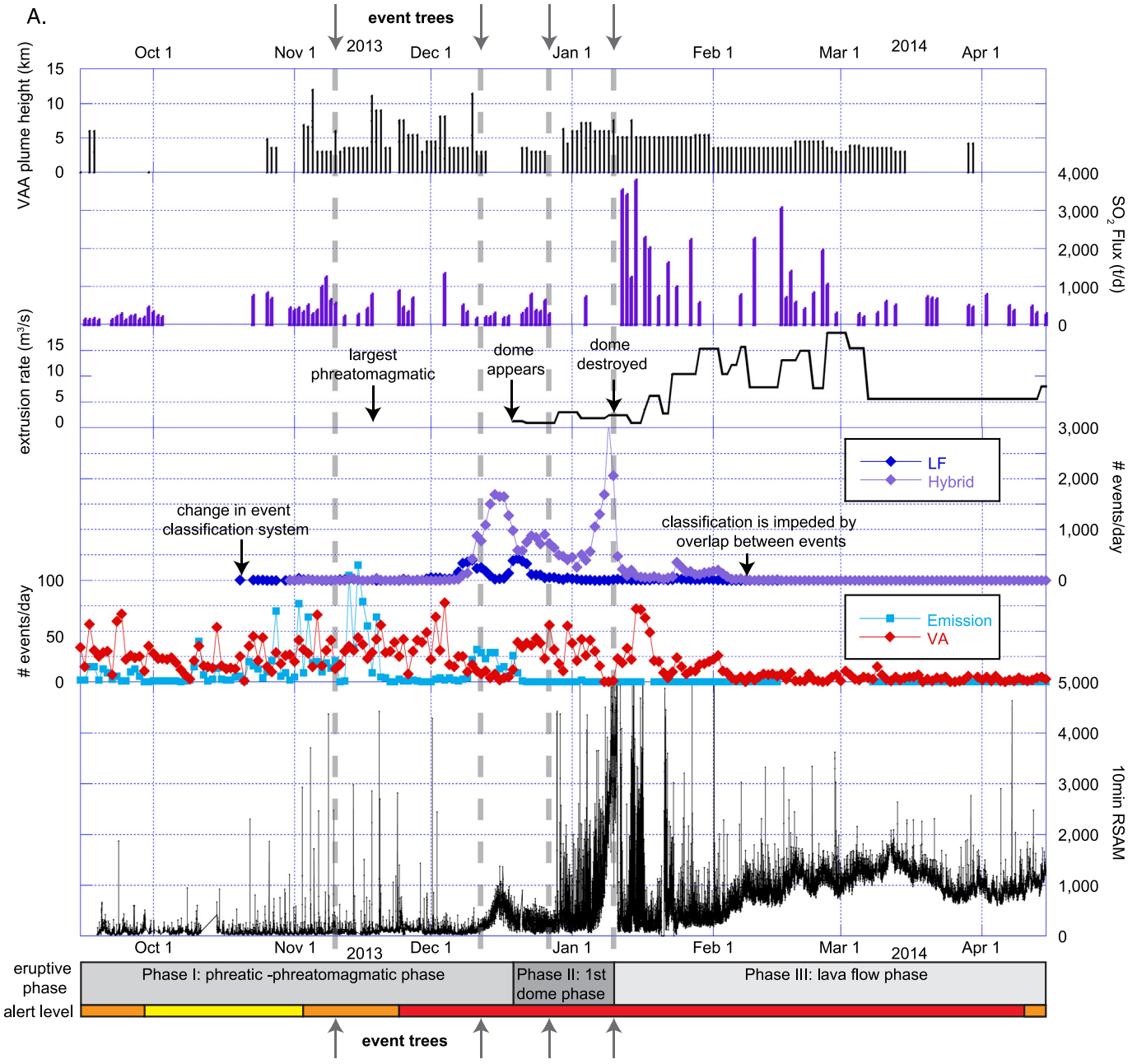

Fig. 3. a and b. Composite graphs of monitoring data between September 15, 2013 and October, 15, 2014. Note that the scale of seismic count information changes between panels a and b. One month of time (March 15 to April 15, 2014) is repeated on both plots for continuity. Volcanic Ash Advisory (VAA) column heights (in km above sea level) do not include some low-level (<4 km) plumes due to cloud cover (Pallister et al. 2019). SO_2 emission rate data is from campaign measurements (Primulyana et al., 2019). Lava extrusion rates are taken from Pallister et al. 2019. Seismic event counts (# events per day) are shown for low frequency (LF), hybrid, VA (distal or deep volcano-tectonic), and emission events (McCausland et al. 2019). 10-minute real-time seismic amplitude (RSAM) data is shown for seismic station Lau Kawar. Also shown are eruptive phases, CVGHM alert levels, and arrows that point to dates of probabilistic event tree forecasts.

were accompanied by PDCs with runout distances between 0.5 and 1.5 km; runout increased to 2 km by early December. Eruption frequency also increased; in the first week of December, there were up to 7 eruptions/day. The SO_2 emission rate continued to be high, reaching a maximum of 1343 tons/day on December 4 (Primulyana et al., 2019) and CO_2-rich gas was recognized at a warm spring on the south side of the volcano. Deep LFs and deep VTs returned on November 29, at which time shallow proximal seismicity began to transition from dominantly VTs to dominantly LFs and hybrids (McCausland et al. 2019). On December 10, LF seismicity and the overall Real-time Seismic Amplitude Measurement (RSAM) value increased at previously unobserved rates with LFs becoming increasingly repetitive in size and inter-event spacing and self-similar in waveform (McCausland et al. 2019). Finally, observations documented movement of the crater rim by as much as 125 m laterally and dilation of up to 10-m-wide radial fractures (Pallister et al. 2019), prompting construction of a second event tree on December 12, 2013.

The occurrence and dominance of hybrid earthquakes is interpreted to indicate the presence of magma at very shallow levels, based on analogy with other systems where regularly repeating hybrids preceded dome extrusion within days to weeks, e.g., at Mount St. Helens and Huila (MSH: Moran et al., 2004, Huila: Cardona et al., 2009). By analogy, we suggested that dome extrusion was highly likely within hours to days. However, we noted the need to evaluate the reliability of this indicator through a more comprehensive look at the global catalog. Given this interpretation, combined with the historic pattern of dome-

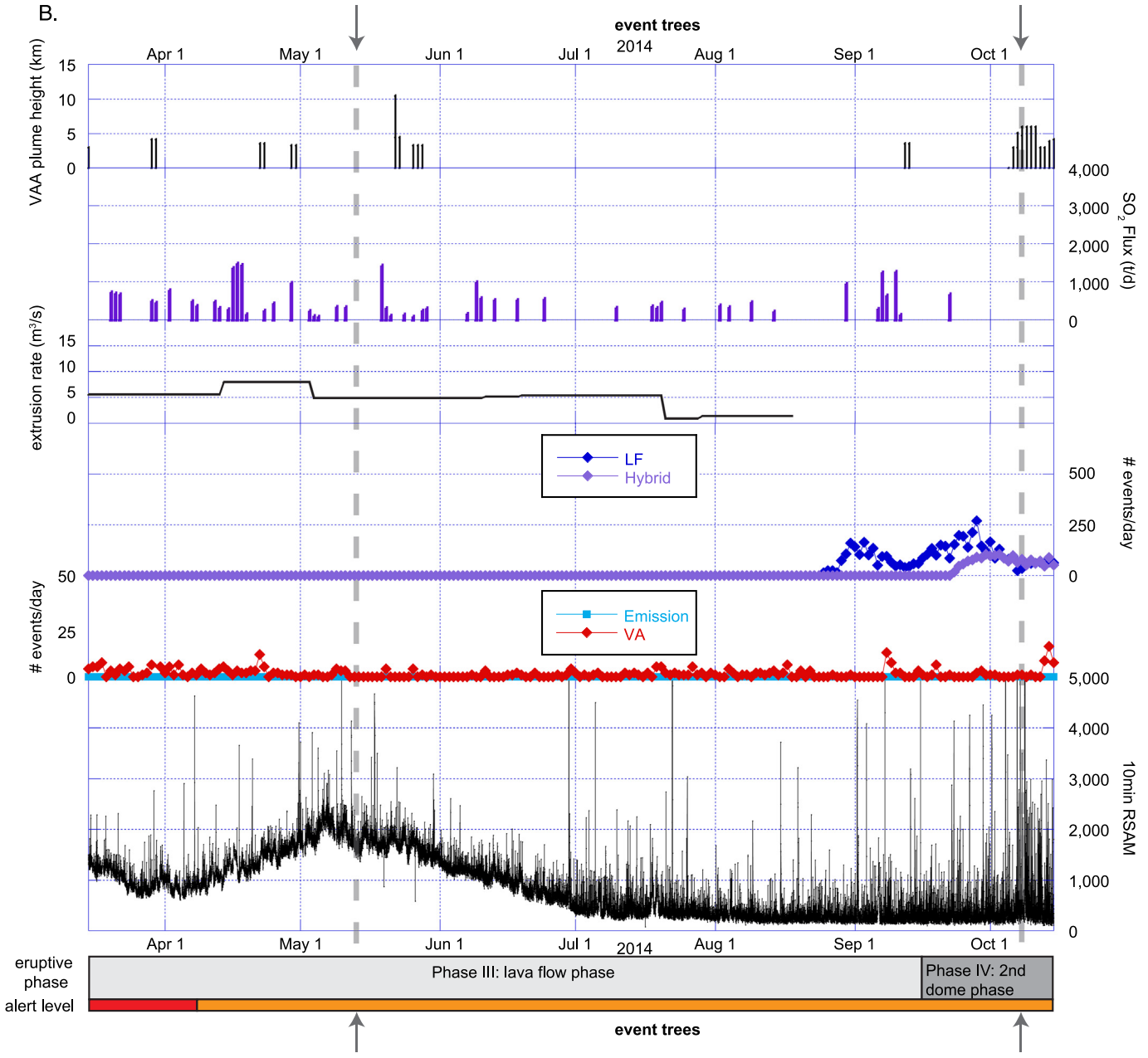

Fig. 3 (*continued*).

forming eruptions, the highest likelihood was assigned to VEI 2–3 events (node 4, Fig. 5).

In addition, the tree limb that was called "Sector collapse ± blast" on the November 7 event tree (nodes 7 & 13, Fig. 4) was changed to "Debris avalanche from summit ± blast" (nodes 7 & 14, Fig. 5). This revision took into account the possibility of partial summit area collapse, as opposed to collapse of major portions of the overall edifice. A relatively high, 30% conditional probability for the debris avalanche scenario was assigned to a VEI > 3 eruption, and a 15% conditional probability was assigned to the debris avalanche scenario for a VEI 2–3 event. These probabilities were highly influenced by the potential for collapse of the part of the summit located between the radial fractures near the NE crater. Such a summit collapse took place at Merapi in 2010 and resulted in a small blast (Komorowski et al., 2013). A broader sector collapse of a large volume of the edifice was regarded as unlikely, but possible, and might have generated a lateral blast, such as that observed in the 1997 event at the Soufriere Hills volcano, Montserrat (Sparks et al., 2002; suggested for Sinabung by Iguchi et al., 2012).

PDC hazard probabilities were estimated using global compilations and the pre-historic record at Sinabung. First, the reference distances (to answer the question: would PDCs surpass × distance?) for PDC travel listed on the event tree changed from 4 km on November 7 to 5 km on December 10. This distance change reflected our concern of larger PDCs and development of the PDC fan. This change and the accompanying discussion among the CVGHM and USGS teams influenced and mirrored expansion of the evacuation zone to 7 km (on November 24, see Discussion section; Fig. 5). Second, probabilities for pyroclastic flow occurrence and runout follow Newhall and Hoblitt (2002) in using the frequency of association between phenomena and magnitude of eruption from the GVP catalog (Simkin and Siebert, 1994). For example, the probability of PDCs in a VEI 1–2 is 5%; probability of PDCs at VEI 3 is 35% (Newhall and Hoblitt, 2002). Third, exceedance probabilities for

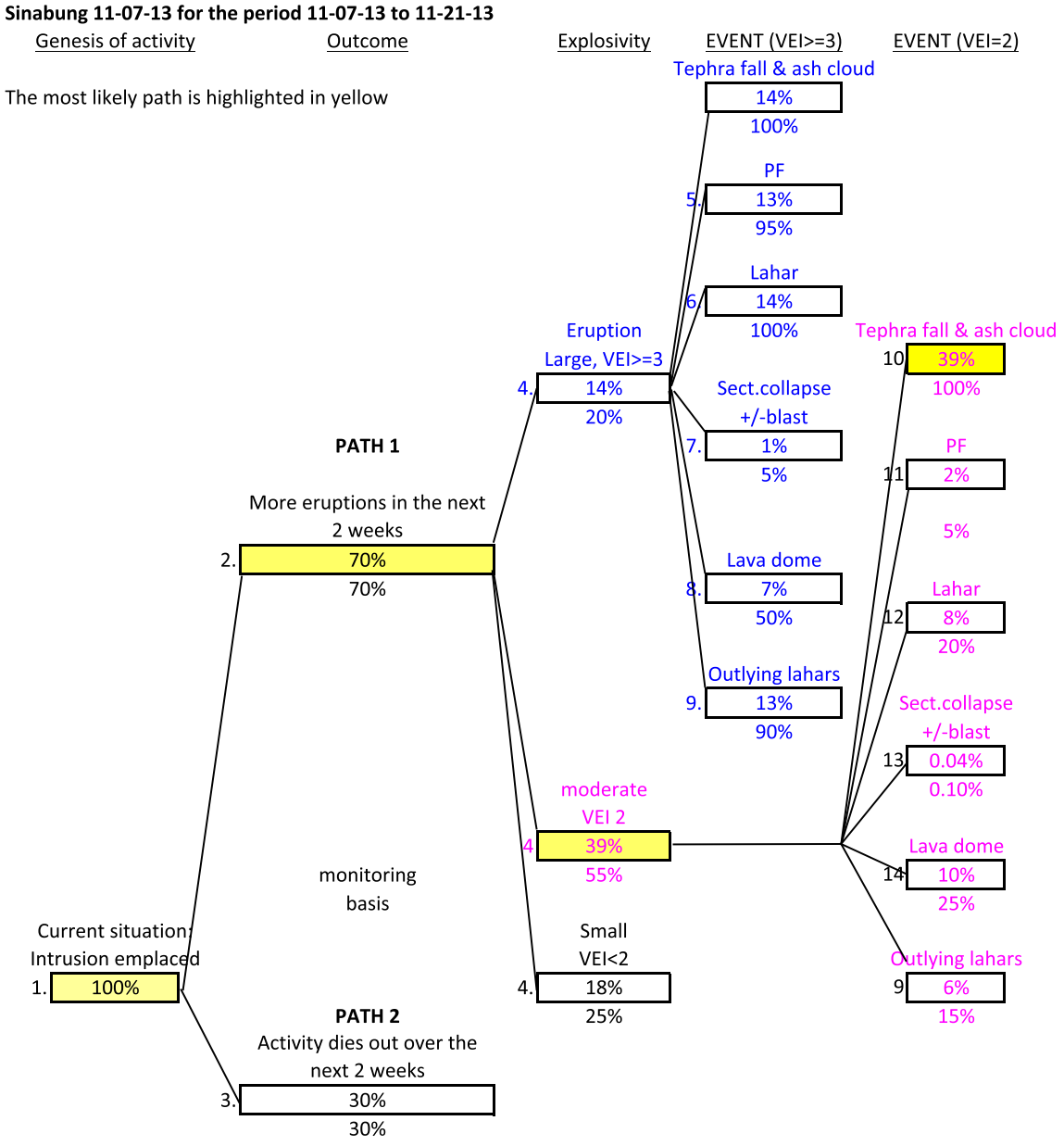

Fig. 4. November 7–10, 2013 event tree for subsequent two weeks of activity at Sinabung volcano. Nodes are numbered and refer to explanatory text that documents the rationale for assignment of conditional probabilities (the probabilities listed below black boxes). Conditional probabilities are multiplied by their parent nodal probabilities (cell within the black box connected via a tieline to the left) to produce nodal probabilities (those within black boxes). The most likely scenario is highlighted in yellow. Different font colors are used to help the reader distinguish between limbs on the tree.

PDC runout also follow Newhall and Hoblitt (2002). Newhall and Hoblitt (2002) compiled eruption VEI, PDC runout, and vertical drop for 191 PDCs, from which they calculate runout exceedance probabilities for each VEI magnitude. For example, a VEI 3 with a vertical drop of 1–1.9 km (Sinabung height is ~1.4 km) has a runout distance of 3.9 km at a 90% exceedance probability (Table 1 of Newhall and Hoblitt, 2002). Furthermore, preserved pre-historic pyroclastic flow and lahar deposits at Sinabung extended to distances of 3 to 5 km from the summit (according to geologic maps of Prambada et al., 2010 and Iguchi et al., 2012). In estimating the probability of PDC runout over the one-month validity of this tree, we took into account the exceedance probabilities described above with information about the current activity, for which the VEI 2–3 events to date had produced PDCs that extended <2 km from the summit. The result of this analysis was the forecast of an 80% conditional (58% nodal) probability of PDCs being restricted to <5 km radius from the vent and a 20% conditional (14% nodal) probability of PDCs exceeding 5 km for a VEI 2–3 event (node 16, Fig. 5).

One final probability change since the November 7 tree was to include an increase in the lahar probability for VEI 2 eruptions to 100%, based on the occurrence of lahars in the eruption sequence up to that time and the recognition of the rainfall-intense climate of Sumatra, Indonesia. This change marked a move away from relying on the global compilation of the GVP catalog for which eruptive phenomena are incompletely populated.

Consistent with the most likely path through the tree (highlighted in yellow, Fig. 5), within the one-month forecast window maximum VEI was 2 (80%/72% conditional/nodal probabilities), and a surface dome appeared (see statement that dome extrusion was likely 'within hours to days'; 90%/65% conditional/nodal probabilities; dome appeared on Dec. 18; Pallister et al. 2019). Pyroclastic density currents continued to reach up to 3 km from the vent, within the 5-km exclusion zone, and

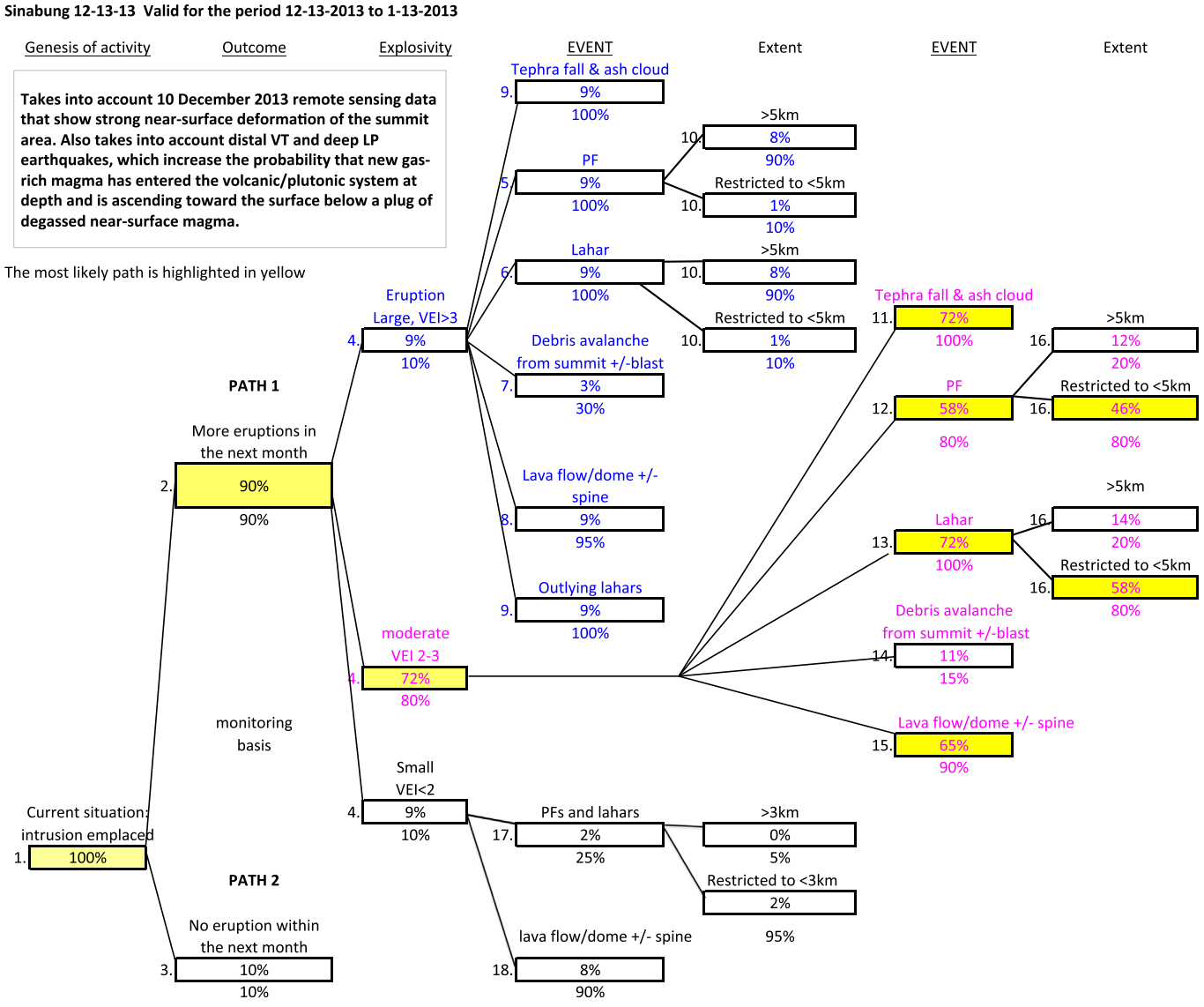

Fig. 5. December 12–14, 2013 event tree for subsequent one month of activity at Sinabung volcano.

consistent with a <5 km highest likelihood (80%/58% conditional/nodal probability) forecast.

3.3. December 27, 2013 tree

Shallow, proximal, repetitive, self-similar LF seismicity peaked on December 14, 2013 (although LF seismicity subsequently increased again in late December, Fig. 3a). On December 16, 2013, shallow, proximal, repetitive, self-similar hybrid seismicity became dominant over LF events, and was followed two days later by the first appearance of an extruded dome on December 18 (Pallister et al. 2019), marking the onset of a new eruptive phase (Phase II, first dome and collapse phase of Gunawan et al. 2019). This dome grew asymmetrically, overtopping the crater wall when its total height reached 50 m on December 26 (Pallister et al. 2019). Based on the presence and height of this dome, another tree was constructed on December 27.

The probability that eruptive activity would continue (though not necessarily every day) over the next month was estimated at 95%, based on the presence of the 50 m high dome at the summit, the opening of fractures near the summit beginning mid-November (Pallister et al. 2019) radial to the NE summit crater, continued tremor, shallow hybrids, LFs, deep LF's, and distal VT's, continued SO_2 emissions in the same range (few hundred to 1500 t/day; Primulyana et al., 2019) as that during the eruptions in November, and continued bubbling of CO_2-rich gas from a warm water spring.

Downlimb probabilities and the tree format were similar to the previous event tree, with the exception of the debris avalanche ± lateral blast scenario. In this tree, separate limbs were included for lateral blast (nodes 8 &15, Fig. 6) and debris avalanche scenarios (nodes 7 & 14, Fig. 6). This distinction was made to highlight the difference between the nature of the two hazards and their relative likelihoods and triggers. The debris avalanche hazard was determined to be high (conditional probability of 75% for VEI > 3 and 15% for VEI 2–3) based on the size and geometry of the growing summit dome and the presence of fractures in the summit area. The blast hazard was determined to be low (5% for VEI > 3; 2% for VEI 2–3), based on the high likelihood for dome collapse and by analogy with Merapi and Soufrière Hills volcanoes (see above).

Finally, the probabilities of PDC occurrence and whether they would surpass reference runout distances began to incorporate results of queries from the DomeHaz and FlowDat databases (Ogburn et al.,

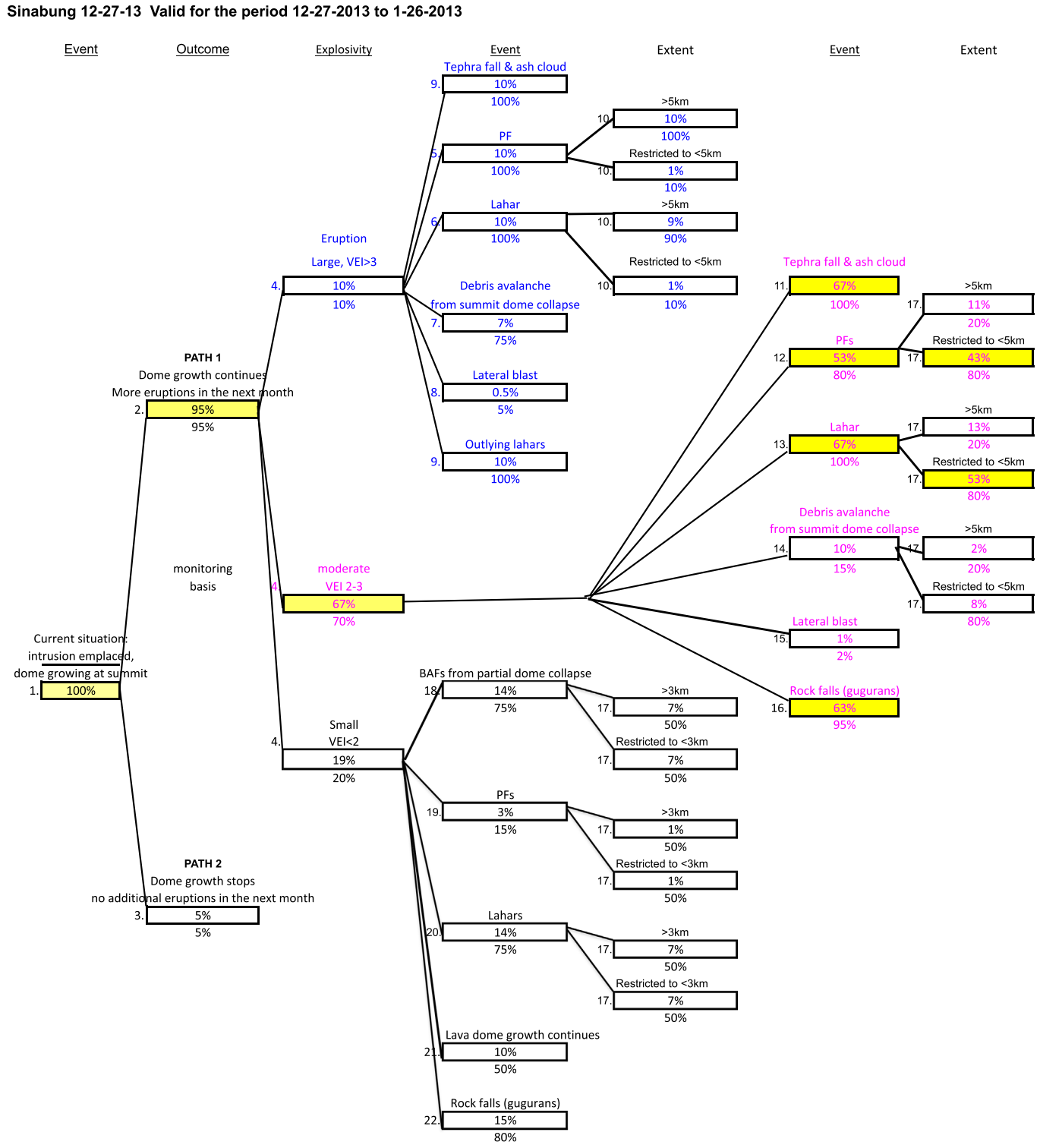

Fig. 6. December 27, 2013 event tree for subsequent one month of activity at Sinabung volcano.

2012, 2015; Ogburn, 2012). For example, from DomeHaz (as of late 2013 version 1.0) 33% of dome-forming eruptions with associated VEI 2 eruptions produced PDCs. However, PDC occurrence data are heavily underreported in the GVP, which DomeHaz v1.0 used to populate associated eruptive phenomena fields. However, activity at Sinabung had already been producing many small PDCs that extended to <3 km from the summit. The conditional probability for PDC occurrence in a VEI 2–3 eruption was therefore set at 80% (node 12, Fig. 6). In retrospect, one could argue that this probability should have been higher, given the presence of a growing dome at the summit. Higher probabilities were considered at the time; however, the team was also well aware of dome-forming eruptions that did not produce PDCs in the first month of dome growth (e.g., Huila, Colombia), and it was argued that another month (duration of this tree) could pass without additional PDCs. Consequently, the consensus of the group was to simply assign a high (80%), but not very high (90%) or near-certain (95%), conditional probability for PDCs within the next month for the VEI 2–3 eruption scenario (node 12, Fig. 6).

Within the one-month forecast window lava extrusion and advance continued, producing explosive dome collapse events with ash columns that rose to over 7 km above sea level, estimated as VEI 2 events, and consistent with the most likely path through the tree. Dome-collapse driven PDCs reached up to 4.5 km from the vent, within the 5 km exclusion zone and within the highest probability PDC runout zone (80% conditional probability for <5 km runout for VEI 2–3 eruptions).

3.4. January 9–10, 2014 tree

RSAM decreased preceding and coincident with dome extrusion beginning mid-December (Fig. 3a). Such decreases in seismic energy have been observed in a number of cases by the VDAP team, and are generally attributed to depressurization of the conduit upon magma reaching the surface (White and McCausland, 2016, 2019). However, in the beginning of January (as documented in the event tree), self-similar hybrid seismicity increased, became increasingly energetic and appeared irregular in time (in hindsight, hybrids did begin to regularize in time again by this point), dominating the seismic record (up to 7 events/min). Also during this time, there was a deep VT, followed by distal VTs (up to M_d 3.6) and one deep LF (M_d 2.3 at ~12 km depth on January 4), indicating pressurization of intermediate levels of the magmatic system and possibly new magma entering the feeding system at greater depth (McCausland et al. 2019; White and McCausland, 2019). Furthermore, minimum and maximum RSAM values were increasing, surpassing the values seen before the appearance of the first dome, and including a five-fold increase in RSAM between January 5 and 9 (McCausland et al. 2019). The dome at the summit inflated, but then deflated in its center, with several surface fractures and repeated margin collapses (Pallister et al. 2019). Taken together, but based largely on seismicity, we assigned a near-certainty (95% conditional probability) for eruption continuation in the subsequent three weeks. We assigned a 5% conditional probability for no further dome growth or eruption, but allowed for continued degassing and phreatic eruptions.

Beyond the eruption continuation vs. cessation fork in the event tree, we reformatted the down-limb structure of the tree, creating non-mutually exclusive branches. This fundamental change was triggered by a change in the nature of the hazard. The growing lava dome was no longer confined to the summit crater and had repeatedly collapsed from flow margins, up to a maximum of 8 times/h on the morning of January 8, 2014 (Pallister et al. 2019; Nakada et al. 2019). As such, pyroclastic flows were not only produced as a result of eruption column collapse (the down-limb consequences of eruptions with varying VEI), but also from destabilization of the dome during non-eruptive periods. To address this distinction, we separated dome collapse events from vent-derived explosions. Each of these branches was then further divided into two different magnitude groups representing small or large collapses, and eruptions similar to or larger than previous events in the sequence (Fig. 7).

The conditional probability that these eruptions would include dome collapse (node 3a, Fig. 7) was set at 100% (95% nodal probability), based on current volcanic activity and the precedent for collapse with the current dome geometry and growth. Within this same time interval, the non-mutually exclusive probability for a vertical eruption from the vent was set at 75% (node 3b, Fig. 7). For the first time in this sequence, we also showed a range of probabilities for this node, reflecting lack of consensus among the group. The probability range extended from 50 to 100% probability, with seismologists favoring a high probability based on evidence for pressurization and lack of regularity in shallow seismicity, and with geologists favoring lower probability of an explosive vent eruption based largely on the past record of eruptive behavior at Sinabung and the possibility that pressure increase could be relieved by lava extrusion. The conditional probability for a large (complete) collapse of this dome to expose the conduit was set at 20% (node 3b, Fig. 7), based largely on observed deflation of the dome and presence of recently opened fractures under the dome, where again a range in values was documented from 10 to 25%. It was hypothesized that such a large collapse would expose and unload the top of the conduit, thereby triggering explosive eruptions, as seen, for example, at Soputan volcano in 2007 (Kushendratno et al., 2012).

The probability distribution for eruption magnitude was again based on global analogs and the current activity. We assigned a conditional probability for VEI > 3 in this tree of 10% (node 3b, Fig. 7). For purposes of this tree, we considered the eruptions of November, with ash plumes of 5–12 km, and the eruption of 10 December 2013, for which the VAAC reported a plume to 38,000′ altitude (11.6 km or ~10 km above the summit) to be VEI 2 eruptions. An estimate of VEI based on plume height alone would put these events in the VEI 3 range; however, convective columns rise to greater heights in the tropics than at higher latitudes (e.g., Tupper et al., 2009) and the relatively small volumes of deposits and the style of eruption were not consistent with VEI 3 (Newhall and Self, 1982). Based mainly on the presence of a surface dome at Sinabung together with previous geologic mapping, and relative probabilities of differing VEIs from the DomeHaz database (Ogburn et al., 2012, 2015), we assigned the highest probability to continued VEI 2 eruptions.

A final change in this tree included the use of the Heim coefficient to approximate pyroclastic flow hazards. We use the Heim coefficient or ΔH/L approximation (where ΔH and L are vertical and horizontal PDC travel distances, respectively, see inset on Fig. 10), because it is a physically based, empirical relationship to estimate pyroclastic flow mobility. Numerous workers (e.g. Heim, 1932; Francis et al., 1974; Hsü, 1975) have noted that an inverse relationship exists between granular mass flow volume and ΔH/L. This relationship has since been applied to characterize pyroclastic flow runout (Sparks, 1976; Hayashi and Self, 1992). Based on this relationship, several authors used ΔH/L to estimate relative pyroclastic flow hazard zones for different pyroclastic flow volumes (e.g., at Soufrière Hills, Montserrat, Wadge and Isaacs, 1988). To achieve this, ΔH/L values are used to produce an energy line that starts at the summit and intersects the topography at a predicted runout distance in the direction of interest (Sheridan, 1979). Using software packages, (cf. Palma, 2013; Takarada, 2013; Schilling, 1998) and a DEM, the energy line concept can be expanded to produce an energy cone that maps on local topography (Fig. 10).

At Sinabung, the total volume of the dome was unknown at the time of tree construction, but had likely reached about 2.8 Mm^3 by January 8 (Pallister et al. 2019) and was even larger by January 10. We approximated ΔH/L between 0.2 and 0.4 (cf. Saucedo et al., 2005), where lower ΔH/L corresponds to larger PDC volumes and/or greater mobility. Furthermore, our calculations of ΔH/L at Sinabung were draped on top of the geologic map of Prambada et al. (2010) for comparison (ΔH/L of 0.2–0.3 shown on Fig. 10). Mapped PDC deposits reach a distance close to the ΔH/L value of 0.3, coincident with an approximate minimum ΔH/L for small volume block and ash flows. This distance also corresponds to the location of the east-west directed Lau Barus, a river valley that may act as a partial topographic barrier (but would not prevent a dilute portion of the PDC from passing). For comparison, an ΔH/L value of 0.2 reaches between 5.6 and 7.9 km from the Sinabung summit. The reference distance for this tree again increased, this time to 7 km in order to reflect the southeast-directed exclusion limit.

And finally, we began to discuss possible eruption duration. Based on the DomeHaz database (Ogburn et al., 2012a), there is a 75% probability that the total duration of extrusion at any volcano would last >39 days (see snapshot of the database in Supplementary data for this event tree).

On the same day that the January 10 event tree was complete, a major collapse of the whole summit dome occurred, an event with a forecast probability of 20%/19% (conditional/nodal). This collapse produced an ash column that rose to 7.5 km and produced PDCs that reached 4.5 km from the summit (Pallister et al. 2019; Fig. 3a). These heights and distances were consistent with the highest probability outcomes in the event tree for this branch. Another low probability event also occurred; a small blast was generated on February 1 (Pallister

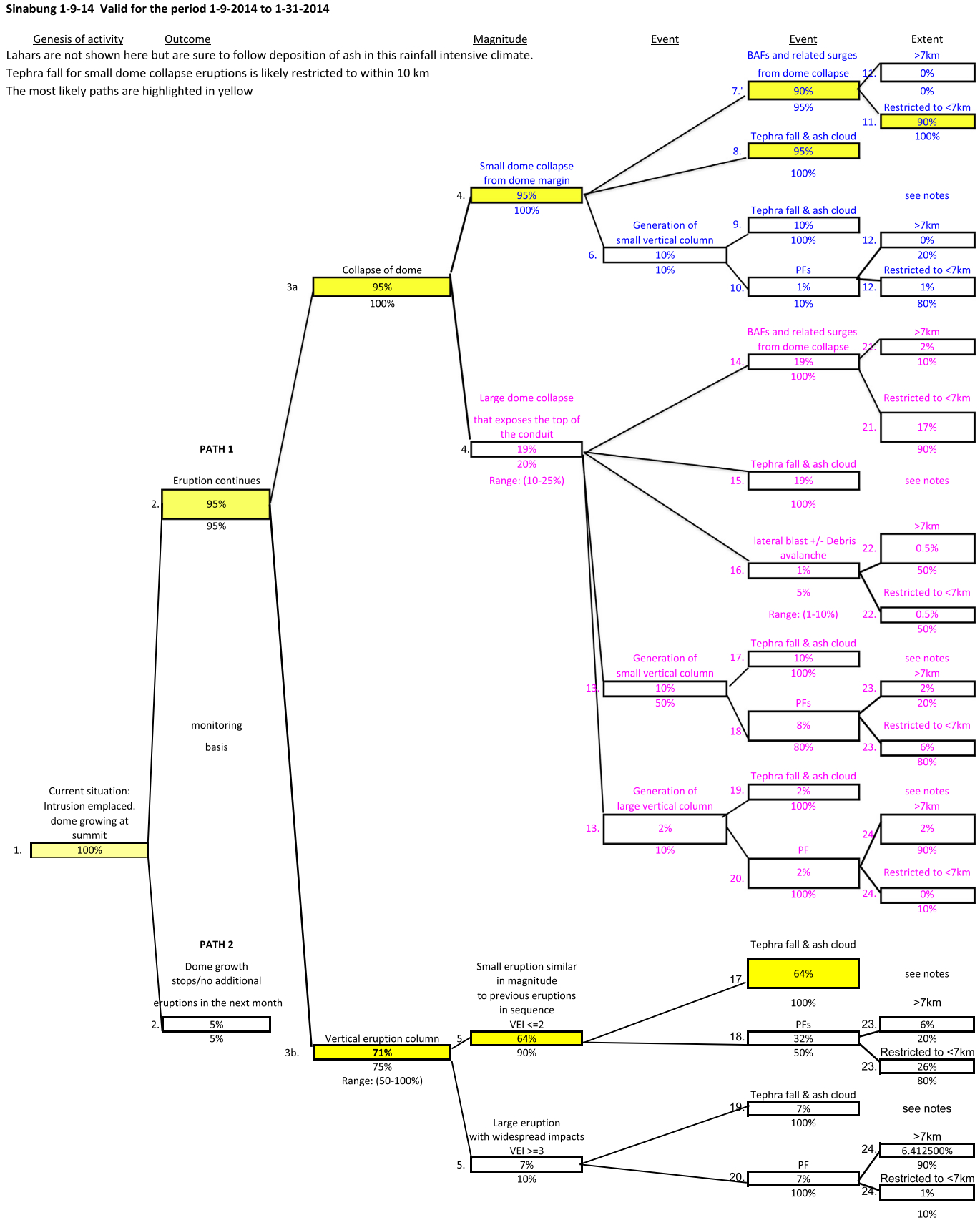

Fig. 7. January 9–10, 2014 event tree for subsequent three weeks of activity at Sinabung volcano. Note that the format of this tree is different than previous trees. The third column here presents scenarios that are not mutually exclusive (dome collapse and vertical eruption column from the vent).

et al. 2019). The forecast for this scenario assigned a 5% conditional and 1% nodal probability of occurrence.

3.5. May 13, 2014 tree

Despite the complete dome collapse and resultant unloading of the conduit on January 10, 2014, there was no change to subsequent vertical eruption columns (limb that includes node 3b of the event tree, Fig. 7). Lava effusion rapidly resumed, producing a lava dome that transitioned into a lava flow down the southeast flank of Sinabung. The January 10 event marked the transition to Phase III, a lava flow and collapse phase of the eruption (Gunawan et al. 2019). This lava flow reached the lower-slope of the volcano by early February 2014 and reached 2.9 km length by October 2014, growing by combined lava flow advance and inflation (Pallister et al. 2019; Nakada et al. 2019). Meanwhile, it experienced frequent flow front and flow margin (particularly on upper southwest side) collapse in January and early February that generated pyroclastic flows to >4 km. A notable collapse occurred on February 1, 2014, generating dense and dilute PDCs that singed trees to 4.9 km from the summit (3.8 km from the collapse site; Pallister et al. 2019). Lava collapse and PDC generation continued at a lower level after early February (Nakada et al. 2019). SO_2 emission rates peaked after the January 10 collapse, but remained high through January and February, then decreased again to pre-dome extrusion rates in March–May. The most recent emission rate measurement before the tree was created was 324 tons/day on May 11, 2014 (Primulyana et al., 2019).

In May 2014, a training workshop was conducted in Garut, Indonesia to introduce methods of event tree construction to CVGHM scientists. In this tree, we removed the non-mutually exclusive branches added in the January 10 tree, including dome collapse and central vent eruptions. The removal of the vertical eruption branch reflected the fact that the complete collapse of the dome on January 10 did not trigger a new phase of vertical eruptions. Instead, branches were added to the lava dome/spine scenario that allowed for either a large or a small collapse, thereby simplifying the tree. During this exercise, participants were divided into two groups, each of which completed population of the same event tree (labeled Group 1 and Group 2 on Fig. 8). In general, the exercise proved a useful way to compare the results of two different groups of scientists, each including a range of disciplinary specialties.

At this point, seismicity had become dominated by emergent, overlapping, regular LF events such that they could not be distinguished as individual events and looked like tremor. Minimum and maximum RSAM values remained elevated above those associated with extrusion of the first dome, but were not unprecedented in the sequence. The likelihood for continued eruptions (though not necessarily continuously) in the next month was again determined to be a near certainty (95%, node 2, Fig. 8), based largely on seismic activity and continued dome growth and collapse. The largest discrepancy between group probabilities was that for eruption magnitude, where the highest probability was either for VEI < 2 or VEI 2–3. Discussion following the exercise revealed that the difference was due to variation in each group's estimation of VEI. The group that called current eruptions VEI 2 placed a high probability on continuing VEI 2–3; those that called current eruptions VEI 1 placed a higher probability on continuing VEI < 2 eruptions.

This group exercise also marked the first longer term forecast, including probabilities that eruption duration would last at least an additional 6 months and 1 year. We used the DomeHaz database (Ogburn et al., 2012) to query dome effusion durations globally. Based on these data, we assessed that there was a 95% conditional probability that the dome duration would continue for another month (at ~8 months since effusion began), an 85% probability that it would last another 6 months, and a 75% probability that it would last another year (note: these probabilities are not shown on Fig. 8 but are in Supplementary material). We further discussed using lava flow volumes as a proxy for effusion duration. The area of the 2014 lava flow at the time of tree construction (2.9 km runout, ~1 km width) was similar to that of other mapped lava flows at the volcano (average 3 km on south side). We posited that, if effusion continually fed a single lava flow in each eruption sequence, the probability for another year of extrusion (which would more than double the volume of the flow if average effusion rate remained constant) was quite low (10–20% here). Finally, by relying on a conceptual model of effusive eruptions in which the end of the eruption is marked by an quasi-exponential decrease in effusion rate and decrease in seismicity with time (e.g., Mount St. Helens 2004-1008, Mastin et al., 2008), we assigned an 80–95% chance it would last at least another month. We relied on the geologic history over the DomeHaz database to assign a 40–60% probability of extrusion lasting another 6 months (beyond its current duration) and a 10–20% probability it would last at least another year.

3.6. October 7, 2014 tree

In mid-September 2014, eruptive activity shifted back to the Sinabung crater, wherein effusion of dome lava caused the first of a new series of collapses with associated ash plumes to 6 km (Phase IV, the second lava dome phase of Gunawan et al. 2019). Lava effusion began at vents on steep slopes near the summit, but did not create a large dome because dome collapses removed mass at about the same rate as extrusion added it. These collapses fed PDCs at an elevated rate (Nakada et al. 2019) that descended along the southwest margin of the 2014 lava flow (Pallister et al. 2019). The maximum PDC runout increased in early October to 5 km.

RSAM peaked in early May, decreasing in minimum and average maximum until July, and then remaining relatively constant after that time (Fig. 3b). In August, LF and hybrid seismicity could once again be distinguished as individual events, rather than looking like tremor. A further change from emergent low frequency earthquakes to more impulsive hybrid earthquakes occurred, and on October 2, a deep/distal VT suggested pressurization of the system at the depth of magma storage. Furthermore, there had been relatively stable SO_2 emissions over the previous few months (last observation mid-September of 672 tons/day; Primulyana et al., 2019), and EDM measurements may have indicated relatively shallow deflation over the preceding week, consistent with longer term deflation measured in one tilt signal (since January), however, other EDM and tilt data did not confirm the same trend. Again, the eruption probability was considered high (95%) for the next month, based largely on seismicity (node 2, Fig. 9). In this tree, we returned to providing a column for extent of PDCs. This was done with reference to the distance to Lau Barus, the river valley that borders the south flank of the volcano. Travel of PDCs or their surge clouds beyond Lau Barus (at 4 to 5 km from the summit on the southeast) would affect more densely populated regions.

Long-term forecasts were also revisited for this event tree (Fig. 9). By October 6, lava effusion had occurred for 292 days. A query of only those dome-forming eruptions that lasted longer than 292 days in the DomeHaz database produced a 95% exceedance probability that extrusion would last at least another month, 70% that it would last >6 months, and 50% chance that it would last >1 year (Ogburn et al., 2012). Therefore, we again assigned a high, 95% probability for eruption lasting another month, but we increased our probability estimates for 6 month and 1 year durations from the last tree (60±20% and 30± 20%, respectively), placing more confidence on the global analog database.

The eruption of Sinabung continued until the time of this writing (May 2017), 3 years after the May 13th event tree was constructed and almost 2.5 years after the October 7th tree. The probability that effusion would last more than one year was estimated to be low at the time of both of these trees (10–20% and 30% in May and October, respectively). In both trees, we relied heavily on a comparison of geologic information (relative size of lava flow) as a proxy for eruption duration rather than the global data from DomeHaz (Ogburn et al., 2012, 2015). However, hindsight shows that this lava flow effectively stopped

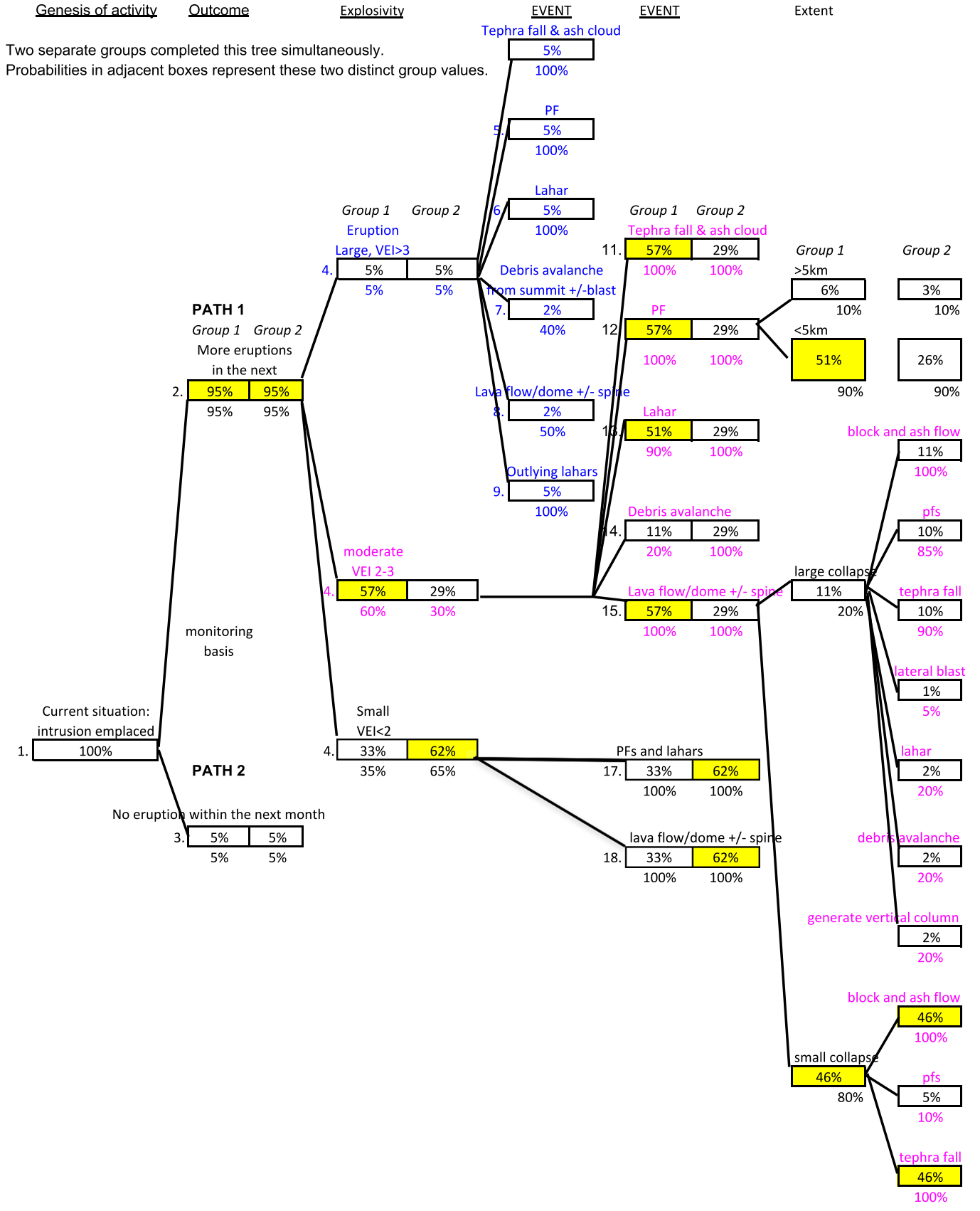

Fig. 8. May 13, 2014 event tree for subsequent one month of activity at Sinabung volcano. Probabilities in this tree were populated by two separate groups of scientists (distinct probabilities labeled 'Group 1' and 'Group 2' here).

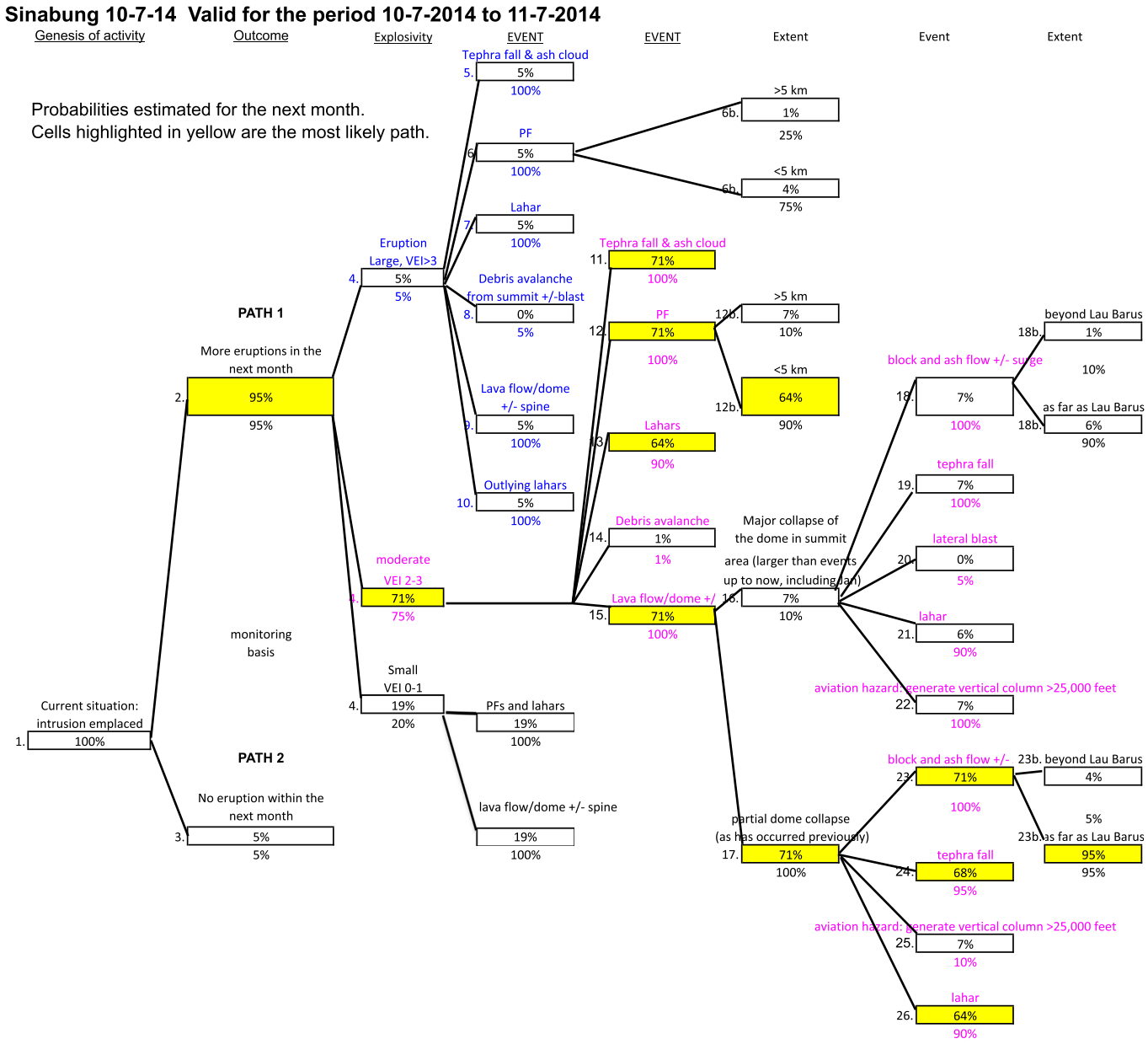

Fig. 9. October 7, 2014 event tree for subsequent one month of activity at Sinabung volcano.

growing at approximately the same time that dome effusion reinitiated at the summit (Phase IV, Gunawan et al. 2019), such that the growth of the lava flow was not a good proxy for total eruption duration. Instead, later estimates of eruption duration estimates were based on global DomeHaz data (see below, using Wolpert et al., 2016).

4. Discussion

4.1. Communication of forecasts

In all cases, communication of event trees highlighted the most likely scenario *and* included mention of less likely but more hazardous scenario(s) (cf. extremity preference, Teigan et al., 2014). Forecasts were communicated between partner agencies VDAP and CVGHM (not to the general public) through a combination of numeric and verbal descriptors. Examples of low probability, elevated hazard events include the debris avalanche and lateral blast scenarios, especially those presented in trees on December 27, 2013 and January 10, 2014. The inclusion of these scenarios reflected the heightened concern caused by observations of cracks opening near the summit, leading to important additions to the tree despite the fact that summit collapse did not occur.

4.2. Dates of alert level/evacuation distance changes

The volcanic alert level changed several times during 2013–5, both increasing and decreasing in response to activity level variation (bottom of Fig. 3). These changes included:

- **September 15**, **2013** 03:00 (WIB): from Levels 2 to 3. At this time, an exclusion zone with a radius of 3 km from the crater was instituted, including the village of Sukameriah.
- **September 29**, **2013** 11:00 from Levels 3 to 2. The exclusion zone decreased to a 2 km radius, while the longer term process of relocating the population of the three closest villages began.

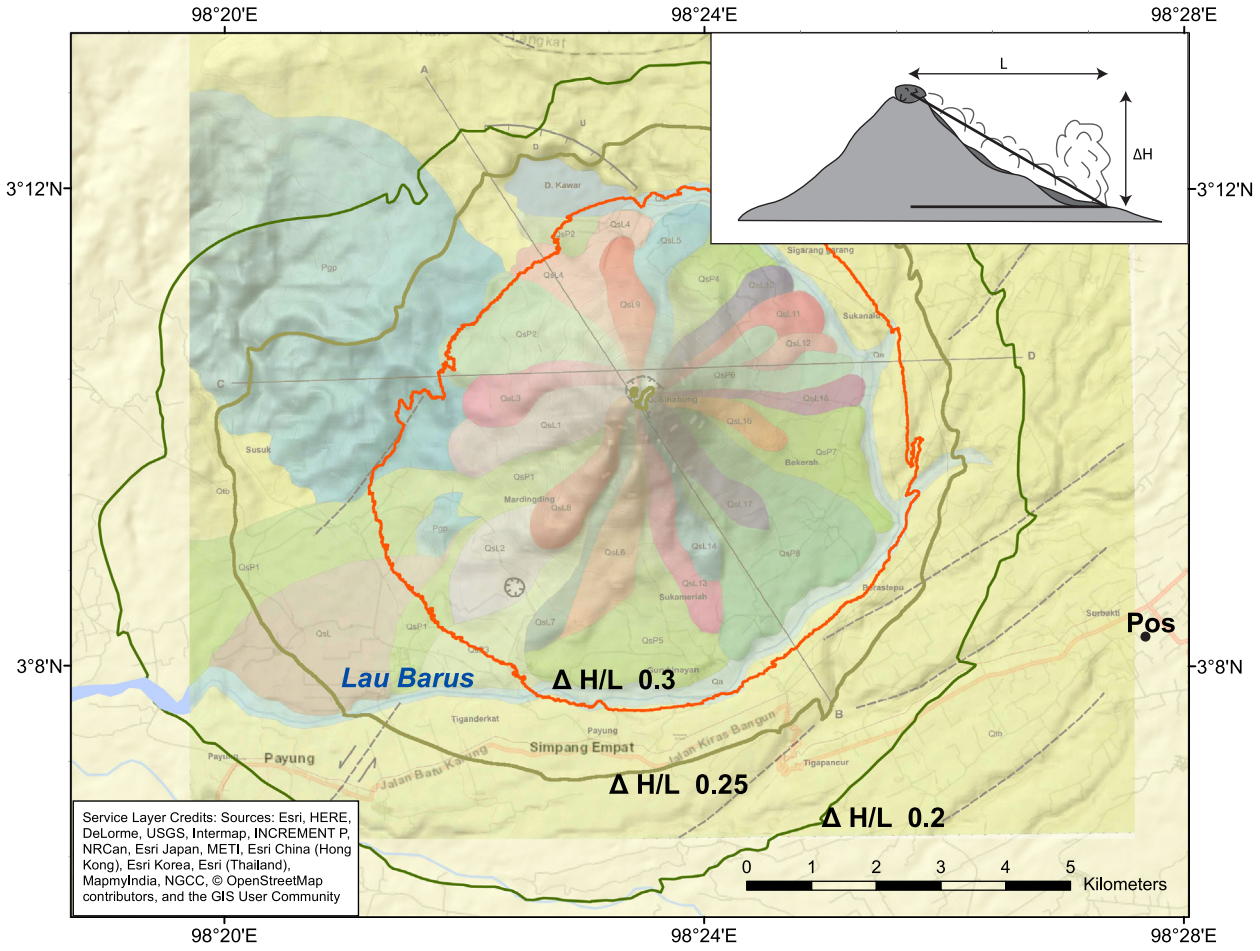

Fig. 10. ΔH/L cones for Sinabung volcano overlain on the geologic map of Prambada et al. (2010). Green and blue units represent pyroclastic flow deposits, whereas red and purple units represent lava flow units on the geologic map. Faults are shown with dashed lines. Note that the Lau Barus (Barus River) runs clockwise around the base of the volcano near the ΔH/L value of 0.3. The point labeled Pos shows the location of CVGHM's observatory post. Inset: cartoon showing ΔH and L runout distances for pyroclastic flow deposits.

- **November 3, 2013** 03:00 from Levels 2 to 3. The exclusion zone again increased to a 3 km radius. Residents in four villages were evacuated.
- **November 24, 2013** 10:00 from Levels 3 to 4. The exclusion radius increased to 5 km. People in 17 villages and 2 hamlets were encouraged to evacuate. People in an additional area beyond 5 km to the southeast were warned about pyroclastic flow hazards. Evacuation remained in effect for the four closest villages. However, by January 10, evacuation was increased to six villages largely to the southeast of the summit.
- **April 8, 2014** 17:00 from Levels 4 to 3. The exclusion radius decreased to 3 km in all directions and to 5 km in sectors to the south and southeast. However, people living outside of this area were allowed to go back to their homes to clean their roofs and perform usual activities. Relocation of residents was prioritized for those living within the exclusion zone and then for those residents within the previous exclusion zone.
- **June 2, 2015** 23:00 from Levels 3 to 4. Since that time, the alert level of the volcano has remained at the highest level AWAS (Level 4; Andreastuti et al. 2019). Over this interval, the hazard map changed twice; the sizes of hazards zones progressively increased through time (Andreastuti et al. 2019). Similarly, evacuation zones increased in size during the eruption, enlarging more in the south and southeast sectors than other sectors based on the likely travel path of lava margin collapse-generated PDCs.

At the time of this writing, ten villages are in evacuation/relocation areas and have suffered severe damage or complete destruction since eruptions began, causing over 9000 people to relocate permanently (Andreastuti et al. 2019). Approximately 5000 families—or nearly 15,800 people—remained displaced as of April 29, 2014, according to the Badan Nasional Penanggulangan Bencana (National Disaster Management Agency). Only two alert level changes occurred within the interval of time covered by event trees presented herein. The November 24, 2013 alert level increase followed the November 7–10 event tree, which forecast a continuation of explosive eruptive activity. However, none of these event trees immediately preceded an alert level change. However, the continued use of event trees for forecasts clarified the current understanding of the magmatic system, highlighting potential important changes in monitoring parameters, and posing questions for desired better understanding of hazard scenarios (see below).

4.3. Progressive improvements/changes in trees

Over the course of this process, we had the opportunity to refine the structure of event trees used for forecasting, to query the literature for possible additional global analogs, and to gather more information about the history and status of Sinabung itself. Here, we highlight some of the improvements in these areas through the course of 2013–4.

4.3.1. Tree structure

Tree format changes were required by the changing nature of the hazards as the eruption progressed. Appearance and growth of a lava

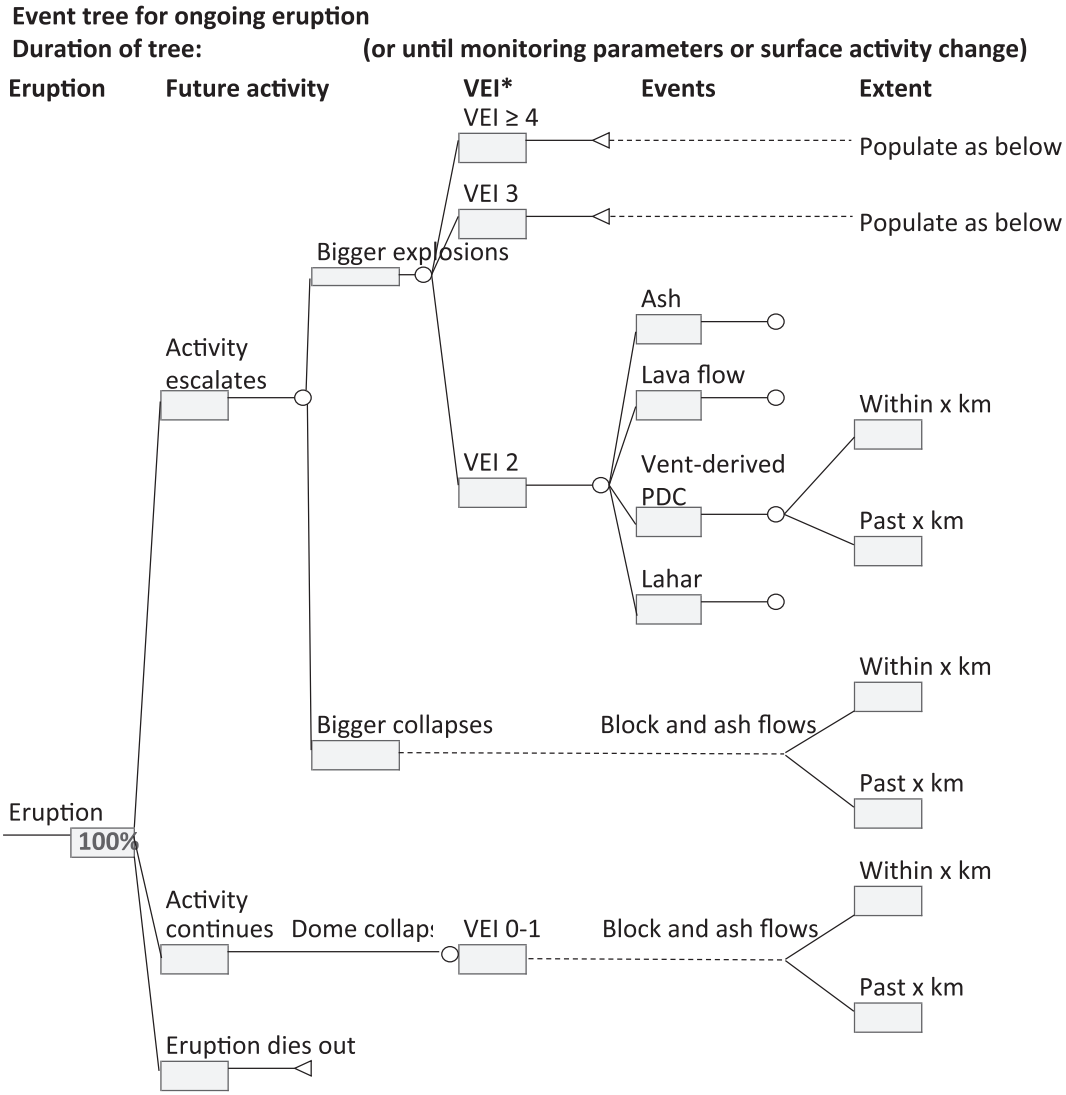

Fig. 11. Generic format of possible future event trees at Sinabung during the current eruptive period, where future activity is framed with reference to current activity. This format is useful, in general, after an eruption has started. The phrase 'block and ash flows' is used represent dome collapse PDCs here, as distinct from 'vent-derived PDCs'.

dome/flow added the possibility for lava margin collapse, which was not dependent upon vent eruption. The addition of a tree branch distinguishing dome/lava collapse is akin to a similar division made in event trees used at the ongoing eruption of Soufriere Hills volcano, Montserrat (Aspinall et al., 2002). However, for Montserrat the branches are mutually exclusive, framed in terms of the first event to occur (dome collapse or vent eruption?) or the largest event over the interval (dome collapse or more explosive vent eruption?). In practice, the non-mutually exclusive format of our tree made it incredibly cumbersome, including so many distinct branches that it became complicated and confusing to read. In order to maintain the distinction between dome collapse and vent-derived activity, we recommend that separate branches be maintained. However, the format can be reframed such that branches are mutually exclusive, where the options include whether activity will be larger, stay the same, or get smaller. A possible structure of this tree is shown in Fig. 11.

4.3.2. Explosivity of eruption

The distribution of VEIs is derived from data from the GVP catalog, which is populated using the maximum VEI of eruption sequences (Global Volcanism Program, 2013). This distribution is certainly biased for several reasons, including under-recording of small volcanic eruptions (e.g., Siebert et al., 2010; Kiyosugi et al., 2015) and the default assignment of VEI 2 to all eruptions that are definitely explosive, but eruption size is not known (though plume height data support relative VEI 2 abundance, Siebert et al., 2010). Even if we could correct for possible under-recording (cf. Furlan, 2010; Mead and Magill, 2014), it is then only an appropriate descriptor of maximum VEI for the entire eruption sequence. In contrast, short-term event trees are framed in terms of a specified time interval that is shorter than the total duration of many eruption sequences. Unfortunately, complete population of all explosive events within an eruption sequence has not been completed, such that calculation of the VEI distribution sampled across appropriate time windows cannot be accomplished. One improvement made across these trees, however, was to compare VEI distribution separately for only dome-forming eruption sequences (from DomeHaz, Ogburn et al., 2012, 2015). Interestingly, this shifts the overall distribution toward higher VEI (22% VEI 0–1; 65% VEI 2; 13% VEI ≥ 3 for all Indonesian eruptions; 6% VEI 0–1; 40% VEI 2; 53% VEI ≥ 3 for all eruptions experiencing dome growth).

VEI branches in these trees also changed format. VEI 2 eruptions were separated out in the first tree, but were later grouped with

VEI 3 events. This change partly reflected the desire to compare future scenarios with current activity. The tree structure put forth in Fig. 11 would also address this point. In addition, definition of VEI for ongoing eruptions was the source of confusion for the event tree workshop exercise in May 2014 and caused discrepancy in the probability results (see above), suggesting that clear definition of terms should be included in tree files, especially when diverse teams are participating.

4.3.3. PDC runout

Early event trees constructed in this sequence relied upon the formulation of Newhall and Hoblitt (2002) to assign probability of PDC and lahar generation from vertical explosive eruptions. After dome extrusion, we switched to the use of energy cones (H/L) to estimate pyroclastic flow runout distances, a significant improvement. Furthermore, the reference distances for pyroclastic flow runout (extent column of event trees; Fig. 2) changed through the trees (what is the probability that PDC runout will surpass 5 km vs. 7 km). The selection of reference distances was largely driven by evacuation zonation. That is, the most useful PDC runout probabilities are framed in terms of risk to human population beyond evacuation limits or beyond large geomorphologic features (e.g., Lau Barus – see discussion in January 9–10, 2014 tree above).

4.3.4. Incorporation of uncertainty

Newhall and Pallister (2014) emphasize the need to improve characterization of uncertainty in the calculation of eruption forecasts in the event tree method used here. The only measure of uncertainty recorded in these trees is the range of values represented in January 10, 2014 and May 13, 2014 trees. In these two instances, differences in assessment between members of the group prevented achievement of consensus. However, no attempt was made to characterize uncertainty for consensus values. As these trees were created during a crisis, for a volcano that had no historic eruptions, and hence, no background monitoring information, there was a need for expediency, transparency and simplicity. The trees were just as important as a structure to guide discussion and reach a consensus among a diverse group of scientists as they were to assign rigorous probabilities. There was also advance agreement that the probabilities assigned would reflect the semi-quantitative opinion of the group and were not intended for quantitative use, such as in loss estimation. We acknowledge that omitting uncertainty analysis poses a problem for such quantitative use; however, existing methods (e.g., Marzocchi and Bebbington, 2012; Aspinall and Cooke, 2013) require extensive background information and pre-establishment of thresholds, or pre-testing of experts, as well as pre-established computer codes to rapidly analyze the data. We concluded that this level of complexity and potential opacity was inappropriate for the situation. However, we hope to improve uncertainty calculations for future trees, perhaps simply by stating confidence bounds for each assigned probability and/or developing or adapting and simplifying existing codes and procedures for expert elicitation.

4.4. Research questions from event tree discussions

Each of these event trees includes documentation of the data and discussions that support subjective assignment of event likelihoods. Also, included in the event tree files are questions about potential global analogs for Sinabung and its activity. Most of these questions require a statistical analysis of large numbers of eruptions and/or non-eruptive unrest periods and their associated monitoring signatures. The existence of these questions and others like them in VDAP event trees from other crises around the world has led to targeted research into using global data by VDAP scientists (cf. Ogburn et al., 2016a). We list some of these questions in italics below and briefly summarize the progress that has been made toward understanding these questions. Further descriptions of recent advances will be presented in subsequent papers. Dates of the event tree from which these questions arose are listed along with some of the questions.

> Dec 12, 2013 What percentage of distal VT swarms are associated with eruption?

White and McCausland (2016) document significant distal VT swarms that precede 111 eruptions at 83 long-dormant stratovolcanoes and intrusions at 21 long dormant stratovolcanoes. The study also found that at least 27 of 35 VEI 4 and greater eruptions since 1955 were preceded by large VTs (≥M5), including 100% of VEI 5 and 6's. Prejean et al. (2015) and Pesicek et al. (2017a) used the beta statistic (Matthews and Reasenberg, 1988) to quantify when distal VT seismicity exceeded the regional background at Alaskan volcanoes and correlated those swarms to intrusions or eruptions. For the Alaskan data, 100% of 4 analyzed VEI 3+ eruptions at long-dormant volcanoes were preceded by significant distal VT swarms, whereas 22% of the nine eruptions with short repose periods were preceded by distal VT swarms. These results do not address the forecasting question useful for event trees. However, Pesicek et al. (2017b) used global seismic catalogs to pose the forward looking question: what percentage of VT earthquakes are followed by eruption? They find that 491 of 15,946, or 3% of large earthquakes (>M4) within 30 km of a Holocene volcano are followed by an eruption within 3 months. Although these results may not have significantly changed our assignment of likelihood for continued eruptions (because eruptions were already under way) on Dec. 12, 2013, they represent a step forward in forecasting utility.

> Dec 27, 2013 What is the average time period of effusive eruption before explosive eruption and what percentage of dome effusions end without explosive eruption? What percent of dome-forming eruptions are associated with VEI's of differing magnitudes? What is the timing of those explosive eruptions?

These questions have been answered or are answerable with the joint use of the DomeHaz (Ogburn et al., 2012, 2015), GVP (Global Volcanism Program, 2013), and EFIS databases (Ogburn et al., 2016a). Ogburn et al., 2015 explored the relationship between large explosions (VEI 4+) and dome growth and investigated the timing of such explosions, the relationship with extrusion rate, and the relationship with magma composition. Large explosions that are associated with dome growth most commonly occur before the onset of dome growth rather than during dome growth or after dome growth ceases (Ogburn et al., 2015), although mafic systems behave differently than more silicic systems (Ogburn et al., 2015; Sheldrake et al., 2016). High extrusion rates also correlate with large explosions. The information about relative timing of large explosions may have prompted us to shift the conditional probability of large eruption (VEI > 3) to lower values in the Dec. 27, 2013 event tree.

> Jan 9–10, 2014 What are VEI – PDC runout distance (or H/L) relationships?

The relationship between VEI and PDC volume (for column collapse PDCs) is not well characterized on a global basis. However, as discussed in the documentation for the January 10th event tree, many workers have found a general inverse relationship between PDC volume and ΔH/L. There have been advances in the energy cone approximation for PDC volumes. The FlowDat database (Ogburn, 2012, 2014) contains data from over 150 PDCs from which linear regressions can give equations for estimating ΔH/L from volume (Ogburn, 2014; Ogburn and Calder, 2017), which can be used to construct energy cones (Malin and Sheridan, 1982) that estimate PDC runout limits over real topography. Furthermore, Ogburn et al. (2016b) developed a method for hierarchical Bayesian modeling of the ΔH/L vs. volume relationship, such that strength can be borrowed from the entire global dataset to reduce

uncertainty when modeling the relationship at individual volcanoes, especially useful where runout distance information is sparse. These advances may have only changed the runout probabilities slightly, but they would have increased confidence in the estimates.

Jan 10, 2014 How does runout change as valleys fill?

While a global analysis of this has not been undertaken, the effects of valley fill or constrictions on PDC flow avulsion from channels have been reported by multiple workers (e.g., Lube et al., 2011; Charbonnier et al., 2013; Ogburn et al., 2014). Increases in mobility have also been noted to have occurred after valley filling (Charbonnier et al., 2013; Ogburn, 2014). Positive correlation between run-out distance and development of pyroclastic fans is also well known to CVGHM geologists, based on their empirical observations of many eruptions. Quantification of this relationship at Sinabung is needed.

Jan 9–10, 2014 What are maximum surge runup heights at various runout distances?

Ogburn et al., 2014 found a distinct relationship between surge detachment, PDC volume, and the cross-sectional area of the valley using data from all dome-collapse PDCs at Soufrière Hills Volcano, Montserrat that remained on land. It was shown that a critical valley cross-sectional area exists below which surges are more likely to spread laterally beyond the dense basal avalanche. The critical cross-sectional area is approximately 1/1000th of block and ash flow volume.

Jan 9–10, 2014 What percentage of VEIs of different magnitude do not produce pyroclastic density currents? e.g., trivial to no pyroclastic density currents produced from Quizapu 1932 (VEI 6; Hildreth and Drake, 1992), Santa Maria 1932 (VEI 5; Williams and Self, 1983), Crater Peak 1992 (1% of eruptive volume in PDCs; Miller et al., 1995), small PDCs at Chaiten 2008 (VEI 4+; Pallister et al., 2013a)

A cursory search of the GVP database shows 63/237 (27%) VEI 5+ events without PDCs, with 12/42 (29%) post-1500C.E. VEI 5+ events without PDCs. Again, these numbers represent only the absence of evidence of PDCs (i.e. a PDC event is not associated with these eruptions in the database). However, answering questions that require evidence of absence (as opposed to merely absence of evidence) from databases can be a challenge, one that can be addressed only for complete catalogs of activity. Therefore this question still remains unanswered.

Jan 9–10, 2014 What are minimum dome/edifice collapse volumes required to produce a lateral blast (cf., Soufriere Hills 1997; Merapi 2010 – Komorowski et al., 2013)?

This question is not resolved.

May 13, 2014 What are dome-forming eruption durations? What are eruption durations for sequences that do not produce a dome?

Using the DomeHaz database (Ogburn et al., 2012, 2015), Wolpert et al., 2016 developed a Bayesian model for estimating the remaining duration of a dome forming eruption based on the current duration of the eruption, and its composition. It was found that after ~ 6 years of activity, it becomes more likely for an eruption to be very long lived (Ogburn et al., 2015b, Wolpert et al., 2016). If the results of this Bayesian model had been available before the May 13, 2014 event tree, we would have calculated that for an eruption that had already lasted 240 days (between September 15, 2013 and May 13, 2014), the median remaining duration would be 2.72 years. This result may have increased our estimate of duration probabilities in the May 13, 2014 event tree, shifting them up from the 40–60% probability of extrusion lasting another 6 months (beyond its current duration) and 10–20% probability it would last at least another year.

May 13 and Oct 7, 2014 Do changes in dome morphology/surface texture precede changes in explosive eruptive behavior? Or do they precede/accompany changes in effusion rate?

Some dome morphology and surface texture information currently exists within the DomeHaz database (Ogburn et al., 2012, 2015) and in observations by the VDAP team, but population is not complete.

5. Closing remarks

Six different event trees were created in 2013–14 for Sinabung volcano, Indonesia. Over that time, the event trees were successful in helping the authors to gather relevant monitoring data, to ask pertinent questions about the magmatic system and possible global analogs, and to highlight the most likely and extreme event scenarios for eruption progression. With each consecutive tree, additional datasets/global analogs were added and analysis broadened. Documentation in the trees reflects these additions, but there is certainly room for additional progress. Event trees created by the VDAP group now document global analogs and model results through addition of extra spreadsheets that contain plots and graphs. Additional documentation is also included, including discussion of the formal translation table between qualitative and quantitative probabilities. Further addition of term definitions could also be included. We further recommend: a) creation of event trees in advance of a crisis, when possible, b) use of the event tree to document both knowns and unknowns, c) creation of consecutive event trees during a crisis to document thought process, d) retrospective looks at event trees (like in this paper) to improve upon methods and inputs for future use. For these trees, the outcomes generally matched the highest probability forecasts and several low probability events also occurred (total dome collapse on January 10 and a small blast on February 1). For all of these reasons, we deem the event tree process a success.

Event trees have been used for eruption forecasting in Indonesia previously. However, this is the first time the event tree method was used so many times during a persistent eruption. The long duration of the ongoing eruption has allowed us to refine and revise our methods, the tree format, and the documentation used to support event trees at Sinabung. Through continued refinement of this process, we can better characterize volcanic hazards at Sinabung, and we can improve the technique so that it can also be used to greater effect elsewhere, as was subsequently done during the Slamet, Indonesia eruption crisis in 2014.

Acknowledgements

The authors acknowledge the Indonesian Geological Agency and its Center for Volcanology and Geologic Hazard Mitigation and the USAID Office of Foreign Disaster Assistance for their support of our work in Sumatra. We appreciate thoughtful reviews from Kyle Anderson, Sarah Ogburn, Natalia Deligne and an anonymous reviewer.

Appendix A. Supplementary data

Supplementary data to this article can be found online at https://doi.org/10.1016/j.jvolgeores.2018.02.003.

References

Andreastuti, S., Paripurno, E., Gunawan, H., Budianto, A., Syahbana, D., Pallister, J., 2019. Character of community response to volcanic crises at Sinabung and Kelud volcanoes. J. Volcanol. Geotherm. Res. 382, 298–310.

Aspinall, W.P., 2006. Structured elicitation of expert judgment for probabilistic hazard and risk assessment in volcanic eruptions. Statistics in Volcanology. 1, pp. 15–30.

Aspinall, W.P., Cooke, R.M., 2013. Quantifying scientific uncertainty from expert judgement elicitation. Risk and Uncertainty Assessment for Natural Hazards, pp. 64–99.

Aspinall, W.P., Loughlin, S.C., Michael, F.V., Miller, A.D., Norton, G.E., Rowley, K.C., Sparks, R.S.J., Young, S.R., 2002. The Montserrat Volcano Observatory: its evolution, organization, role and activities. Geol. Soc. Lond. Mem. 21, 71–91.

Cardona, C., Santacoloma, C., White, R., McCausland, W., Trujillo, N., Narvaez, A., Bolaños, R., Manzo, O., 2009. Sismicidad tip "drumbeat" asociada a la erupción y emplazamiento de un domo en el Volcano Nevado del Huila, Noviembre de 2008. Memorias XII Congreso Colombiano de Geología, pp. 7–11.

Charbonnier, S.J., Germa, A., Connor, C.B., Gertisser, R., Preece, K., Komorowski, J.-C., Lavigne, F., Dixon, T., Connor, L., 2013. Evaluation of the impact of the 2010 pyroclastic density currents at Merapi volcano from high-resolution satellite imagery, field investigations and numerical simulations. J. Volcanol. Geotherm. Res. 261:295–315. https://doi.org/10.1016/j.jvolgeores.2012.12.021.

Doyle, E.E., McClure, J., Johnston, D.M., Paton, D., 2014. Communicating likelihoods and probabilities in forecasts of volcanic eruptions. J. Volcanol. Geotherm. Res. 272, 1–15.

Francis, P.W., Roobol, M.J., Walker, G.P.L., Cobbold, P.R., Cowards, M., 1974. The San Pedro and San Pablo volcanoes of northern Chile and their hot avalanche deposits. Geol. Rundsch. 63 (1):357–388. https://doi.org/10.1007/BF01820994.

Furlan, C., 2010. Extreme value methods for modelling historical series of large volcanic magnitudes. Stat. Model. 10 (2), 113–132.

Global Volcanism Program, 2013. In: Venzke, E. (Ed.), Volcanoes of the World, v. 4.2.2. Smithsonian Institution https://doi.org/10.5479/si.GVP.VOTW4-2013 (Accessed Dec. 2013).

Gunawan, H., Surono, Budianto, A., Kristianto, Prambada, O., McCausland, W., Pallister, J., Iguchi, M., 2019. Overview of the eruptions of Sinabung eruption, 2010 and 2013–present. J. Volcanol. Geotherm. Res. 382, 103–119.

Hayashi, J.N., Self, S., 1992. A comparison of pyroclastic flow and debris avalanche mobility. J. Geophys. Res. 97 (B6):9063. https://doi.org/10.1029/92JB00173.

Heim, A., 1932. Bergsturz und Menschenleben. Fretz and Wasmuth, Zürich.

Hendrasto, M., Surono, Budianto, A., Kristianto, Triastuty, H., Haerani, N., Basuki, A., Suparman, Y., Primulyana, S., Prambada, O., Loeqman, A., Indrastuti, N., Andreas, A.S., Rosadi, U., Adi, S., Iguchi, M., Ohkura, T., Nakada, S., Yoshimoto, M., 2012. Evaluation of volcanic activity at Sinabung volcano, after more than 400 years of quiet. J. Disaster Res. 7, 37–47.

Hildreth, W., Drake, R.E., 1992. Volcán Quizapu, Chilean Andes. Bull. Volcanol. 54 (2), 93–125.

Hsü, K.J., 1975. Catastrophic debris streams (Sturzstroms) generated by rockfalls. Geol. Soc. Am. Bull. 86:129. https://doi.org/10.1130/0016-7606(1975), 86-129.

Iguchi, M., Ishihara, K., Surono, Hendrasto, M., 2011. Learn from 2010 eruptions at Merapi and Sinabung volcanoes in Indonesia. Disaster Prev. Res. Inst. Annu. B 54, 185–194.

Iguchi, M., Nishimura, T., Hendrasto, M., Rosadi, U., Ohkura, T., Triastuty, H., Basuki, A., Loeqman, A., Maryanto, S., Ishihara, K., Yoshimoto, M., 2012. Methods for eruption prediction and hazard evaluation at Indonesian volcanoes. J. Disaster Res. 7 (1), 26–36.

Kiyosugi, K., Connor, C., Sparks, R.S., 2015. How many explosive eruptions are missing from the geologic record? Analysis of the quaternary record of large magnitude explosive eruptions in Japan. J. Appl. Volcanol. 4 (1), 17.

Komorowski, J.C., Jenkins, S., Baxter, P.J., Picquout, A., Lavigne, F., Charbonnier, S., ... Budi-Santoso, A., 2013. Paroxysmal dome explosion during the Merapi 2010 eruption: processes and facies relationships of associated high-energy pyroclastic density currents. J. Volcanol. Geotherm. Res. 261, 260–294.

Kushendratno, Pallister, J.S., Bina, F.R., McCausland, W., Carn, S., Haerani, N., Griswold, J., Keeler, R., 2012. Recent explosive eruptions and volcano hazards at Soputan volcano—a basalt stratovolcano in north Sulawesi, Indonesia. Bull. Volcanol. 74, 1581–1609.

Lindsay, J., Marzocchi, W., Jolly, G., Constantinescu, R., Selva, J., Sandri, L., 2010. Towards real-time eruption forecasting in the Auckland Volcanic Field: application of BET_EF during the New Zealand National Disaster Exercise 'Ruaumoko'. Bull. Volcanol. 72 (2), 185–204.

Lube, G., Cronin, S.J., Thouret, J.-C., 2011. Kinematic characteristics of pyroclastic density currents at Merapi and controls on their avulsion from natural and engineered channels. Geol. Soc. Am. Bull. 123 (5–6):1127–1140. https://doi.org/10.1130/B30244.1.

Malin, M.C., Sheridan, M.F., 1982. Computer-assisted mapping of pyroclastic surges. Science 217 (4560):637–640. https://doi.org/10.1126/science.217.4560.637.

Marzocchi, W., Bebbington, M.S., 2012. Probabilistic eruption forecasting at short and long time scales. Bull. Volcanol. 74 (8), 1777–1805.

Marzocchi, W., Sandri, L., Gasparini, P., Newhall, C., Boschi, E., 2004. Quantifying probabilities of volcanic events: the example of volcanic hazard at Mount Vesuvius. J. Geophys. Res. 109, B11201. https://doi.org/10.1029/2004JB003155.

Mastin, L.G., Roeloffs, E., Beeler, N.M., Quick, J.E., 2008. Constraints on the size, overpressure, and volatile content of the Mount St. Helens magma system from geodetic and dome-growth measurements during the 2004–2006+ eruption. A Volcano Rekindled: The Renewed Eruption of Mount St. Helens, 2004–2006, pp. 461–478.

Mastrandrea, M.D., Mach, K.J., Plattner, G.K., Edenhofer, O., Stocker, T.F., Field, C.B., Ebi, K.L., Matschoss, P.R., 2011. The IPCC AR5 guidance note on consistent treatment of uncertainties: a common approach across the working groups. Clim. Chang. 108, 675–691.

Matthews, M.V., Reasenberg, P.A., 1988. Statistical methods for investigating quiescence and other temporal seismicity patterns. Pure Appl. Geophys. 126 (2), 357–372.

McCausland, W., White, R., Indrastuti, N., Gunawan, H., Patria, C., Suparman, Y., Putra, A., Triastuty, H., Hendrasto, M., 2019. Using a process-based model of pre-eruptive seismic patterns to forecast evolving eruptive styles at Sinabung Volcano, Indonesia. J. Volcanol. Geotherm. Res. 382, 253–266.

Mead, S., Magill, C., 2014. Determining change points in data completeness for the Holocene eruption record. Bull. Volcanol. 76 (11), 874.

Miller, T.P., Neal, C.A., Waitt, R.B., 1995. Pyroclastic flows of the 1992 Crater Peak eruptions: distribution and origin. The 1992 eruptions of Crater Peak vent, Mount Spurr Volcano, Alaska. U.S. Geol. Surv. Bull. 2139, 81–87.

Moran, S.C., Malone, S.D., Qamar, A.I., Thelen, W.A., Wright, A.K., Caplan-Auerbach, J., 2004. Seismicity associated with renewed dome building at Mount St. Helens, 2004–2005. A volcano rekindled: the renewed eruption of Mount St. Helens, 2006. U.S. Geological Survey Professional Paper 1750, pp. 27–60.

Nakada, S., Zaennudin, A., Yoshimoto, M., Maeno, F., Suzuki, Y., Hokanishi, N., Sasaki, H., Iguchi, M., Ohkura, T., Gunawan, H., Triastuty, H., 2019. Growth process of the lava dome/flow complex at Sinabung Volcano during 2013–2016. J. Volcanol. Geotherm. Res. 382, 120–136.

Neri, A., Aspinall, W.P., Cioni, R., Bertagnini, A., Baxter, P.J., Zuccaro, G., Andronico, D., Barsotti, S., Cole, P.D., Ongaro, T.E., Hincks, T.K., 2008. Developing an event tree for probabilistic hazard and risk assessment at Vesuvius. J. Volcanol. Geotherm. Res. 178 (3), 397–415.

Newhall, C.G., 1982. A method for estimating intermediate- and long-term risk from volcanic activity, with an example from Mount St. Helens, Washington. U.S. Geological Survey Open-File Report, pp. 82–396.

Newhall, C., Hoblitt, R., 2002. Constructing event trees for volcanic crises. Bull. Volcanol. 64 (1), 3–20.

Newhall, C.G., Pallister, J.S., 2015. Using multiple data sets to populate probabilistic volcanic event trees. Volcanic Hazards Risks Disasters, pp. 203–232.

Newhall, C.G., Self, S., 1982. The volcanic explosivity index (VEI) an estimate of explosive magnitude for historical volcanism. J. Geophys. Res. Oceans 87, 1231–1238.

Ogburn, S.E., 2012. FlowDat—mass flow database: Vhub database. available at. https://vhub.org/groups/massflowdatabase.

Ogburn, S.E., 2014. Reconciling Field Observations of Pyroclastic Density Currents with Conceptual and Computational Analogs Using a GIS and a Newly Developed Global Database. SUNY at Buffalo (PhD Dissertation, 318 pp.).

Ogburn, S.E., Calder, E.S., 2017. The relative effectiveness of empirical and physical models for simulating pyroclastic density currents under different emplacement conditions. Front. Earth Sci. 5 (83). https://doi.org/10.3389/feart.2017.00083.

Ogburn, S.E., Loughlin, S.C., Calder, E.S., 2012. DomeHaz—dome-forming eruptions database v2.4: Vhub database. available at. https://vhub.org/groups/domedatabase.

Ogburn, S.E., Calder, E.S., Cole, P., Stinton, A.J., 2014. The effect of topography on ash-cloud surge generation and subsequent flow propagation. In: Wadge, G., Robertson, R.E.A., Voight, B. (Eds.), The Eruption of Soufriere Hills Volcano, Montserrat From 2000 to 2010. Geological Society, London, Memoirs. 39:pp. 177–192. https://doi.org/10.1144/M39.10.

Ogburn, S.E., Loughlin, S., Calder, E.S., 2015. The association of lava dome growth with major explosive activity (VEI ≥ 4): DomeHaz, a global dataset. Bull. Volcanol. 77: 1–17. https://doi.org/10.1007/s00445-015-0919-x.

Ogburn, S.E., Harpel, C.J., Pesicek, J.D., Wellik, J., Pallister, J.S., Wright, H.M., 2016a. Using global data for eruption forecasting. U.S. Geological Survey Open File Report 2016-1104.

Ogburn, S.E., Berger, J.O., Calder, E.S., Lopez, D., Patra, A.K., Pitman, E.B., Rutarindwa, R., Spiller, E.T., Wolpert, R.L., 2016b. Pooling strength amongst limited datasets using hierarchical Bayesian analysis, with application to pyroclastic density current mobility metrics. Statistics in Volcanology. 2:pp. 1–26. https://doi.org/10.5038/2163-338X.2.1.

Pallister, J., Diefenbach, A., Burton, W., Muñoz, J., Griswold, J., Lara, L., Lowenstern, J., Valenzuela, C., 2013a. The Chaitén rhyolite lava dome: eruption sequence, lava dome volumes, rapid effusion rates and source of the rhyolite magma: Andean. Geology 40 (2):277–294. https://doi.org/10.5027/andgeoV40n2-a06.

Pallister, J.S., Schneider, D.J., Griswold, J.P., Keeler, R.H., Burton, W.C., Noyles, C., Newhall, C.G., Ratdomopurbo, A., 2013b. Merapi 2010 eruption—chronology and extrusion rates monitored with satellite radar and used in eruption forecasting. J. Volcanol. Geotherm. Res. 261, 144–152.

Pallister, J., Wessels, R., Griswold, J., McCausland, W., Kartadinata, N., Gunawan, H., Budianto, A., Primulyana, S., 2019. Monitoring, forecasting collapse events, and mapping pyroclastic deposits at Sinabung volcano with satellite imagery. J. Volcanol. Geotherm. Res. 382, 149–163.

Palma, J.L., 2013. Energy cone. https://vhub.org/resources/econe.

Pesicek, J., Ogburn, S., Wellik, J., 2017a. Toward a Global Assessment of Patterns in Precursory and Eruptive Seismicity for Improved Eruption Forecasting. IAVCEI General Assembly, Portland, Oregon.

Pesicek, J., Wellik, J., Prejean, S., 2017b. Assessing the Likelihood of an Impending Eruption Using the Distal VT Model and the Catalog of Alaskan Volcanic Eruptions.

Prambada, O., Zaennudin, A., Iryanto, Basuki, A., Yulius, C., Mulyadi, Rohaeti, E., Kisroh, Suparmo, 2010. Report of Geological Mapping of Sinabung Volcano, Regency of Karo, Province of North Sumatera. Center for Volcanology and Geological Hazard Mitigation (Unpublished report (in Indonesian)).

Prejean, S.G., Pesicek, J.D., Wellik, J., Cameron, C., White, R.A., McCausland, W.A., Buurman, H., 2015. Eruption forecasting in Alaska: a retrospective and test of the distal VT model. American Geophysical Union Fall Meeting. AGU Fall Meeting Abstracts (abstract #V14B-03).

Primulyana, S., Kern, C., Lerner, A., Saing, U., Kunrat, S., Alfianti, H., Marlia, M., 2019. Gas and ash emissions associated with the 2010–present activity of Sinabung Volcano, Indonesia. J. Volcanol. Geotherm. Res. 382, 184–196.

Saucedo, R., Macías, J.L., Sheridan, M.F., Bursik, M.I., Komorowski, J.C., 2005. Modeling of pyroclastic flows of Colima Volcano, Mexico: implications for hazard assessment. J. Volcanol. Geotherm. Res. 139 (1), 103–115.

Schilling, S.P., 1998. LAHARZ; GIS programs for automated mapping of lahar-inundation hazard zones. U.S. Geological Survey Open-File Report 98-638 (79 pp.).

Sheldrake, T.E., Sparks, R.S.J., Cashman, K.V., Wadge, G., Aspinall, W.P., 2016. Similarities and differences in the historical records of lava dome-building volcanoes: implications for understanding magmatic processes and eruption forecasting. Earth Sci. Rev. 160, 240–263.

Sheridan, M.F., 1979. Emplacement of pyroclastic flows: a review. Geol. Soc. Am. Spec. Pap. 180, 125–136.

Siebert, L., Simkin, T., Kimberly, P., 2010. Volcanoes of the World. Univ of California Press.

Simkin, T., Siebert, L., 1994. Volcanoes of the World: A Regional Directory, Gazetteer, and Chronology of Volcanism During the Last 10,000 Years. Geoscience Press (349 pp.).
Sparks, R.S.J., 1976. Grain size variations in ignimbrites and implications for the transport of pyroclastic flows. Sedimentology 23 (2):147–188. https://doi.org/10.1111/j.1365-3091.1976.tb00045.x.
Sparks, R.S.J., Barclay, J., Calder, E.S., Herd, R.A., Komorowski, J.C., Luckett, R., Norton, G.E., Ritchie, L.J., Voight, B., Woods, A.W., 2002. Generation of a debris avalanche and violent pyroclastic density current on 26 December (Boxing Day) 1997 at Soufriere Hills Volcano, Montserrat. Geol. Soc. Lond. Mem. 21 (1), 409–434.
Takarada, S., 2013. G-EVER activities and the next-generation volcanic hazard assessment system. AGU Fall Meeting Abstracts (abstract #NH43C-03).
Teigan, K.H., Juanchich, M., Filkuková, P., 2014. Verbal probabilities: an alternative approach. Q. J. Exp. Psychol. 67 (1), 124–146.
Tupper, A., Textor, C., Herzog, M., Graf, H.F., Richards, M.S., 2009. Tall clouds from small eruptions: the sensitivity of eruption height and fine ash content to tropospheric instability. Nat. Hazards 51 (2), 375–401.
Wadge, G., Isaacs, M.C., 1988. Mapping the volcanic hazards from Soufriere Hills Volcano, Montserrat, West Indies using an image processor. J. Geol. Soc. 145 (4), 541–551.
White, R., McCausland, W., 2016. Volcano-tectonic earthquakes: a new tool for estimating intrusive volumes and forecasting eruptions. J. Volcanol. Geotherm. Res. 309, 139–155.
White, R.A., McCausland, W.A., 2019. A process-based model of pre-eruption seismicity patterns and its use for eruption forecasting at dormant stratovolcanoes. J. Volcanol. Geotherm. Res. 382, 267–297.
Williams, S.N., Self, S., 1983. The October 1902 plinian eruption of Santa Maria volcano, Guatemala. J. Volcanol. Geotherm. Res. 16 (1–2), 33–56.
Wolpert, R.L., Ogburn, S.E., Calder, E.S., 2016. The longevity of lava dome eruptions. J. Geophys. Res. 121:676–686. https://doi.org/10.1002/2015JB012435.